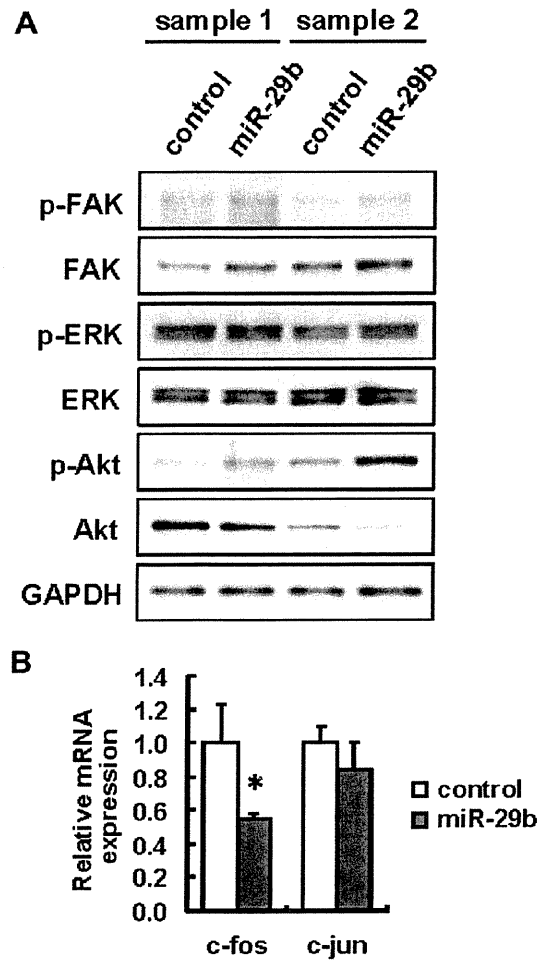

Fig. 3. Effects of miR-29b overexpression on the ECM- and growth factor-related signaling in mouse primary HSCs. Mouse HSCs were transfected with 10 nM miR-29b precursor or a negative control (control) on Day 1 and were incubated for 3 days. (A) Phosphorylation of FAK (Y397), ERK (T202/Y204) and Akt (S473) was analyzed by Western blot. (B) mRNA expression levels of c-fos and c-jun were analyzed by real-time PCR. The results are expressed as relative expression against the expression of control. $^*P < 0.05$ compared with control.

increased the cell number up to 1.7 times that of the non-treated cells (Fig. 2E), whereas overexpression of miR-29b inhibited this increase. Furthermore, in LX-2 cells, transfection of the miR-29b precursor decreased cell viability to 89% and 81% at 3 and 5 days following transfection, respectively (Fig. 2F). These results suggested that miR-29b is able to suppress the proliferation of HSCs and that down-regulation of miR-29b during HSC activation may contribute to their active proliferation.

3.4. Effects of miR-29b overexpression on the ECM- and growth factor-related signaling in primary mouse HSCs

The question of how miR-29b functions in blocking HSC activation was also examined. We showed that overexpression of miR-29b suppressed Col1a1, Col1a2, FN1, DDR2, ITGB1, and PDGFR-β expression (Fig. 2A and B). DDR2 is a receptor tyrosine kinase that is activated by the binding of collagen and was reported to be involved in the proliferation of HSCs and in the expression of matrix metalloproteinase-2 [15,16]. ITGB1 is a member of the integrin family and works as a FN or collagen receptor by forming a heterodimer with the integrin α subunit. ITGB1 is reported to be involved in the production of type I collagen and monocyte chemotactic protein-1 in HSCs [17,18]. PDGFR-β is a receptor of PDGF and is involved in the proliferation of activated HSCs [19,20]. Because it is known that intracellular signaling molecules such as FAK, ERK, and PI3K/Akt are key mediators for DDR2, ITGB1, and PDGFR-β [14,21–24], their down-regulation by miR-29b may affect downstream signaling, resulting in the inhibition of both activation and proliferation of HSCs. To verify this hypothesis, we investigated the effect of miR-29b overexpression on the activation of FAK, Akt, and ERK. Activation of these kinases was evaluated by immunoblot analyses to detect the phosphorylation of each protein. Unexpectedly, phosphorylation of FAK, ERK, and Akt was unaffected by miR-29b overexpression (Fig. 3A). Next, we also examined the mRNA expression of c-fos and c-jun, which form the transcription factor AP-1 complex and are located downstream of these signal kinases. Although transfection of the miR-29b precursor failed to alter c-jun expression, it significantly reduced c-fos mRNA expression to 55% (Fig. 3B). Because AP-1 is known to be one of the key transcription factors for the initiation of HSC activation [25,26], this fact indicates that effects of miR-29b may be partially mediated by c-fos down-regulation.

4. Conclusion

We confirmed that miR-29b expression decreased during HSC activation and found that overexpression of miR-29b is able to attenuate the activation and trans-differentiation of HSCs, although the precise molecular mechanism for this effect remains unknown. Changes in miR-29b expression seem to profoundly affect the activation of HSCs.

Conflict of interest

The authors have no conflict of interest to declare.

Acknowledgment

This work was supported by a grant from the Ministry of Health, Labor and Welfare of Japan to N. Kawada (2008–2010).

References

[1] R. Bataller, D.A. Brenner, Hepatic stellate cells as a target for the treatment of liver fibrosis, Semin. Liver Dis. 21 (2001) 437–451.
[2] S.L. Friedman, Molecular regulation of hepatic fibrosis an integrated cellular response to tissue injury, J. Biol. Chem. 275 (2000) 2247–2250.
[3] D.P. Bartel, MicroRNAs: genomics, biogenesis, mechanism, and function, Cell 116 (2004) 281–297.
[4] C.J. Guo, Q. Pan, B. Jiang, G.Y. Chen, D.G. Li, Effects of upregulated expression of microRNA-16 on biological properties of culture-activated hepatic stellate cells, Apoptosis 14 (2009) 1331–1340.
[5] C.J. Guo, Q. Pan, D.G. Li, H. Sun, B.W. Liu, miR-15b and miR-16 are implicated in activation of the rat hepatic stellate cell: an essential role for apoptosis, J. Hepatol. 50 (2009) 766–778.
[6] J.L. Ji, J.S. Zhang, G.C. Huang, J. Qian, X.Q. Wang, S. Mei, Over-expressed microRNA-27a and 27b influence fat accumulation and cell proliferation during rat hepatic stellate cell activation, FEBS Lett. 583 (2009) 759–766.
[7] S.K. Venugopal, J. Jiang, T.H. Kim, Y. Li, S.S. Wang, N.J. Torok, J. Wu, M.A. Zern, Liver fibrosis causes downregulation of miRNA-150 and miRNA-194 in hepatic stellate cells, and their overexpression causes decreased stellate cell activation, Am. J. Physiol. Gastrointest. Liver Physiol. 298 (2010) G101–G106.
[8] Y. Sekiya, T. Ogawa, M. Iizuka, K. Yoshizato, K. Ikeda, N. Kawada, Down-regulation of cyclin E1 expression by microRNA-195 accounts for interferon-β-induced inhibition of hepatic stellate cell proliferation, J. Cell. Physiol. 2010, doi:10.1002/jcp22598.
[9] T. Ogawa, M. Iizuka, Y. Sekiya, K. Yoshizato, K. Ikeda, N. Kawada, Suppression of type I collagen production by microRNA-29b in cultured human stellate cells, Biochem. Biophys. Res. Commun. 391 (2010) 316–321.
[10] C. Roderburg, G.W. Urban, K. Bettermann, M. Vucur, H. Zimmermann, S. Schmidt, J. Janssen, C. Koppe, P. Knolle, M. Castoldi, F. Tacke, C. Trautwein, T. Luedde, Micro-RNA profiling reveals a role for miR-29 in human and murine liver fibrosis, Hepatology 53 (2011) 209–218.

[11] N. Uyama, L. Zhao, E. Van Rossen, Y. Hirako, H. Reynaert, D.H. Adams, Z. Xue, Z. Li, R. Robson, M. Pekny, A. Geerts, Hepatic stellate cells express synemin, a protein bridging intermediate filaments to focal adhesions, Gut 55 (2006) 1276–1289.

[12] L. Xu, A.Y. Hui, E. Albanis, M.J. Arthur, S.M. O'Byrne, W.S. Blaner, P. Mukherjee, S.L. Friedman, F.J. Eng, Human hepatic stellate cell lines, LX-1 and LX-2: new tools for analysis of hepatic fibrosis, Gut 54 (2005) 142–151.

[13] D.M. Bissell, D. Roulot, J. George, Transforming growth factor beta and the liver, Hepatology 34 (2001) 859–867.

[14] F. Marra, M. Pinzani, R. Defranco, G. Laffi, P. Gentilini, Involvement of phosphatidylinositol 3-kinase in the activation of extracellular signal-regulated kinase by PDGF in hepatic stellate cells, FEBS Lett. 376 (1995) 141–145.

[15] E. Olaso, K. Ikeda, F.J. Eng, L.M. Xu, L.H. Wang, H.C. Lin, S.L. Friedman, DDR2 receptor promotes MMP-2-mediated proliferation and invasion by hepatic stellate cells, J. Clin. Invest. 108 (2001) 1369–1378.

[16] E. Olaso, J.P. Labrador, L.H. Wang, K. Ikeda, F.J. Eng, R. Klein, D.H. Lovett, H.C. Lin, S.L. Friedman, Discoidin domain receptor 2 regulates fibroblast proliferation and migration through the extracellular matrix in association with transcriptional activation of matrix metalloproteinase-2, J. Biol. Chem. 277 (2002) 3606–3613.

[17] F. Marra, S. Pastacaldi, R.G. Romanelli, M. Pinzani, P. Ticali, V. Carloni, G. Laffi, P. Gentilini, Integrin-mediated stimulation of monocyte chemotactic protein-1 expression, FEBS Lett. 414 (1997) 221–225.

[18] D.R. Wang, M. Sato, L.N. Li, M. Miura, N. Kojima, H. Senoo, Stimulation of pro-MMP-2 production and activation by native form of extracellular type I collagen in cultured hepatic stellate cells, Cell Struct. Funct. 28 (2003) 505–513.

[19] E. Borkham-Kamphorst, J. Herrmann, D. Stoll, J. Treptau, A.M. Gressner, R. Weiskirchen, Dominant-negative soluble PDGF-beta receptor inhibits hepatic stellate cell activation and attenuates liver fibrosis, Lab. Invest. 84 (2004) 766–777.

[20] C.G. Lechuga, Z.H. Hernandez-Nazara, E. Hernandez, M. Bustamante, G. Desierto, A. Cotty, N. Dharker, M. Choe, M. Rojkind, PI3K is involved in PDGF-beta receptor upregulation post-PDGF-BB treatment in mouse HSC, Am, J. Physiol. Gastrointest. Liver Physiol. 291 (2006) G1051–G1061.

[21] V. Carloni, R.G. Romanelli, M. Pinzani, G. Laffi, P. Gentilini, Focal adhesion kinase and phospholipase C gamma involvement in adhesion and migration of human hepatic stellate cells, Gastroenterology 112 (1997) 522–531.

[22] C. Rodriguez-Juan, P. de la Torre, I. Garcia-Ruiz, T. Diaz-Sanjuan, T. Munoz-Yague, E. Gomez-Izquierdo, P. Solis-Munoz, J.A. Solis-Herruzo, Fibronectin increases survival of rat hepatic stellate cells – a novel profibrogenic mechanism of fibronectin, Cell. Physiol. Biochem. 24 (2009) 271–282.

[23] H.J. Wu, Z.Q. Zhang, B. Yu, S. Liu, K.R. Qin, L.A. Zhu, Pressure activates Src-dependent FAK–Akt and ERK1/2 signaling pathways in rat hepatic stellate cells, Cell. Physiol. Biochem. 26 (2010) 273–280.

[24] K. Ikeda, L.H. Wang, R. Torres, H. Zhao, E. Olaso, F.J. Eng, P. Labrador, R. Klein, D. Lovett, G.D. Yancopoulos, S.L. Friedman, H.C. Lin, Discoidin domain receptor 2 interacts with Src and Shc following its activation by type I collagen, J. Biol. Chem. 277 (2002) 19206–19212.

[25] R. Gao, D.K. Ball, B. Perbal, D.R. Brigstock, Connective tissue growth factor induces c-fos gene activation and cell proliferation through p44/42 MAP kinase in primary rat hepatic stellate cells, J. Hepatol. 40 (2004) 431–438.

[26] J.E. Poulos, J.D. Weber, J.M. Bellezzo, A.M.D. Bisceglie, R.S. Britton, B.R. Bacon, J.J. Baldassare, Fibronectin and cytokines increase JNK, ERK, AP-1 activity, and transin gene expression in rat hepatic stellate cells, Am. J. Physiol. 273 (1997) G804–G811.

Journal of Cellular Physiology

Down-Regulation of Cyclin E1 Expression by MicroRNA-195 Accounts for Interferon-β-Induced Inhibition of Hepatic Stellate Cell Proliferation

YUMIKO SEKIYA,[1,2] TOMOHIRO OGAWA,[1,2] MASASHI IIZUKA,[1,2] KATSUTOSHI YOSHIZATO,[1,2,3] KAZUO IKEDA,[4] AND NORIFUMI KAWADA[1,2]*

[1]*Department of Hepatology, Graduate School of Medicine, Osaka City University, Osaka, Japan*

[2]*Liver Research Center, Graduate School of Medicine, Osaka City University, Osaka, Japan*

[3]*PhoenixBio Co. Ltd., Hiroshima, Japan*

[4]*Department of Anatomy and Cell Biology, Graduate School of Medical Sciences, Nagoya City University, Aichi, Japan*

Recent studies have suggested that interferons (IFNs) have an antifibrotic effect in the liver independent of their antiviral effect although its detailed mechanism remains largely unknown. Some microRNAs have been reported to regulate pathophysiological activities of hepatic stellate cells (HSCs). We performed analyses of the antiproliferative effects of IFNs in HSCs with special regard to microRNA-195 (miR-195). We found that miR-195 was prominently down-regulated in the proliferative phase of primary-cultured mouse HSCs. Supporting this fact, IFN-β induced miR-195 expression and inhibited the cell proliferation by delaying their G1 to S phase cell cycle progression in human HSC line LX-2. IFN-β down-regulated cyclin E1 and up-regulated p21 mRNA levels in LX-2 cells. Luciferase reporter assay revealed the direct interaction of miR-195 with the cyclin E1 3′UTR. Overexpression of miR-195 lowered cyclin E1 mRNA and protein expression levels, increased p21 mRNA and protein expression levels, and inhibited cell proliferation in LX-2 cells. Moreover miR-195 inhibition restored cyclin E1 levels that were down-regulated by IFN-β. In conclusion, IFN-β inhibited the proliferation of LX-2 cells by delaying cell cycle progression in G1 to S phase, partially through the down-regulation of cyclin E1 and up-regulation of p21. IFN-induced miR-195 was involved in these processes. These observations reveal a new mechanistic aspect of the antifibrotic effect of IFNs in the liver.

J. Cell. Physiol. 226: 2535–2542, 2011.

Hepatic fibrosis is characterized by excessive accumulation of extracellular matrices (ECM) and is a common feature of chronic liver diseases. Hepatic stellate cells (HSCs) are considered to play multiple roles in the fibrotic process. HSCs maintain a quiescent phenotype and store vitamin A under physiological conditions. When liver injury occurs, they become activated and trans-differentiate into myofibroblastic cells, whose characteristics include the proliferation, loss of vitamin A droplets, expression of α-smooth muscle actin (α-SMA), secretion of profibrogenic mediators and ECM (Friedman, 2000; Bataller and Brenner, 2001). Therefore, controlling the population and activation of HSCs should be a potential therapeutic target against liver fibrosis.

Interferons (IFNs) are cytokines with antiviral, immunomodulatory, and cell growth inhibitory effects. IFN-α and -β are classified as type I IFNs (Pestka et al., 1987; Uze et al., 2007), which are generally applied for the therapy of eradication of hepatitis B and C viruses. Studies using rodent models and cultured HSCs have also suggested that IFNs have a direct antifibrotic potential independently of their antivirus activity (Mallat et al., 1995; Fort et al., 1998; Shen et al., 2002; Inagaki et al., 2003; Chang et al., 2005; Tanabe et al., 2007; Ogawa et al., 2009), although the detailed molecular mechanisms of these effects of IFNs remain to be clarified.

Recently, microRNAs (miRNAs), which are endogenous small non-coding RNA, have become a focus of interest as post-transcriptional regulators of gene expression through interaction with the 3′ untranslated region (3′UTR) of target mRNAs (Bartel, 2004). miRNAs are known to participate in cell proliferation, development, differentiation, and metabolism (Bartel, 2004). Moreover, it has been reported that expression of miRNAs could alter hepatic pathophysiology; microRNA-122 (miR-122) is involved in the IFN-β-related defense system against viral hepatitis C (Pedersen et al., 2007), and miR-26 is associated with survival and response to adjuvant IFN-α therapy in patients with hepatocellular carcinoma (HCC) (Ji et al., 2009a). Regarding HSCs, miR-15b and miR-16 are down-regulated upon HSC's activation, and their overexpression induces apoptosis and a delay in the cell cycle (Guo et al., 2009a,b). Knockdown of miR-27a and miR-27b in activated HSCs allowed a switch to a more quiescent phenotype and decreased cell proliferation (Ji et al., 2009b). miR-150 and miR-194 suppress proliferation, activation, and ECM production of HSCs (Venugopal et al., 2010). Recently, we showed that miR-29b was induced by IFN and suppressed type I collagen production in LX-2 cells (Ogawa et al., 2010).

In the present study, we measured the levels of miR-195 in primary-cultured mouse HSCs and found that its expression was markedly reduced in their activation phase, suggesting the regulatory role of miR-195 in the activation/deactivation process of

Contract grant sponsor: The Ministry of Health, Labour and Welfare of Japan;
Contract grant number: 2008-KAKEN-IPPAN-003.

*Correspondence to: Norifumi Kawada, Department of Hepatology, Graduate School of Medicine, Osaka City University, 1-4-3, Asahimachi, Abeno, Osaka 545-8585, Japan.
E-mail: kawadanori@med.osaka-cu.ac.jp

Received 6 September 2010; Accepted 3 December 2010

Published online in Wiley Online Library (wileyonlinelibrary.com), 29 December 2010.
DOI: 10.1002/jcp.22598

TABLE 1. Sequences of primers used in real-time PCR analyses and 3'UTR cloning for luciferase reporter assay

Gene	Accession no.	Sequence
Real-time PCR		
CDK2	NM_001798	Forward: 5'-CTCCACCGAGACCTTAAACCTCAG-3' Reverse: 5'-TCGGTACCACAGGGTCACCA-3'
CDK4	NM_000075	Forward: 5'-GATAGATGCTGACCCATACCTCAAG-3' Reverse: 5'-ATGCTGTGGTGCTTTGAGGTAG-3
CDK6	NM_001259	Forward: 5'-ATATCTGCCTACAGTGCCCTGTCTC-3' Reverse: 5'-GTGGGAATCCAGGTTTTCTTTGCAC-3'
Cyclin E1	NM_001238	Forward: 5'-GCAGTATCCCCAGCAAATC-3' Reverse: 5'-TCAAGGCAGTCAACATCCA-3'
Cyclin D1	NM_053056	Forward: 5'-GCTGTGCATCTACACCGACAACTC-3' Reverse: 5'-AGGTTCCACTTGAGCTTGTTCACC-3'
E2F3	NM_001949	Forward: 5'-CCAACTCAGGACATAGCGATTGCTC-3' Reverse: 5'-AGGAATTTGGTCCTCAGTCTGCTGT-3'
GAPDH	NM_002046	Forward: 5'-GCACCGTCAAGGCTGAGAAC-3' Reverse: 5'-TGGTGAAGACGCCAGTGGA-3'
p21	NM_000389	Forward: 5'-AGCAGAGGAAGACCATGTGGA-3' Reverse: 5'-GGAGTGGTAGAAATCTGTCATGCT-3'
p27	NM_004064	Forward: 5'-AGCTTGCCCGAGTTCTACTACAG-3' Reverse: 5'-ACCAAATGCGTGTCCTCAGAGT-3'
3'UTR cloning		
Cyclin E1	NM_001238	Forward: 5'-TTCTCGAGATCCTTCTCCACCAAAGACAGTT-3' Reverse: 5'-TTTCTAGAGAATGGATAGATATAGCAGCACTTACA-3'

The forward and reverse primers for 3'UTR cloning carried the *Xho*I and *Xba*I sites at their 5'-ends, respectively.

HSCs. Because miR-195 is categorized into the same family as miR-15b and miR-16 and has been reported to regulate cell cycle by targeting E2F3, CDK6, and cyclin D1 (Xu et al., 2009), we suspect the involvement of miR-195 in the proliferation of HSC and in type I IFN, in particular IFN-β, -induced inhibition of their growth.

Materials and Methods

Materials

Human HSC line LX-2 was donated by Dr. Scott L. Friedman (Mount Sinai School of Medicine, New York, NY) (Xu et al., 2005). Necessary reagents and materials were obtained from the

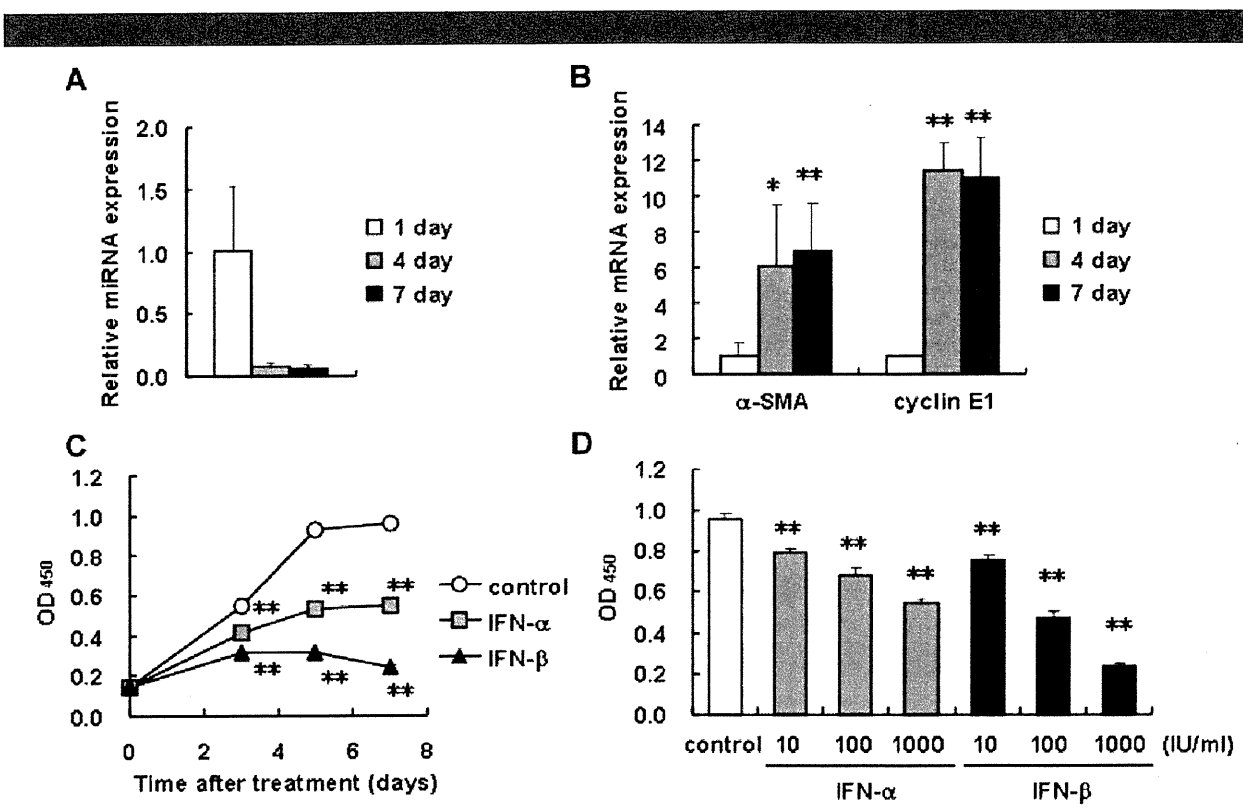

Fig. 1. Expression of miR-195 in mouse HSCs during primary culture and growth inhibitory effect of IFN-α and -β on human stellate cells. A,B: Isolated mouse HSCs were cultured for the indicated periods. The expression levels of miR-195 (A), and α-SMA and cyclin E1 mRNA (B) were measured by real-time PCR. *$P < 0.05$, **$P < 0.01$ compared with 1 day. C,D: LX-2 cells were incubated with IFN-α or -β (1,000 IU/ml) for 3–7 days (C), or with IFN-α or -β at the concentration of 10–1,000 IU/ml for 7 days (D). Control indicates non-treated cells. The proportion of viable cells was determined using a WST-1 assay. **$P < 0.01$ compared with control.

following sources: Dulbecco's modified Eagle's medium (DMEM) from Sigma Chemical Co. (St. Louis, MO); fetal bovine serum (FBS) from Invitrogen (Carlsbad, CA); human natural IFN-α and -β from Otsuka Pharmaceutical Co. (Tokushima, Japan) and Toray Industries, Inc. (Tokyo, Japan), respectively; precursor and inhibitor of miR-195, and the corresponding negative controls from Ambion (Austin, TX); mouse monoclonal antibody against cyclin E1, cyclin D1 and p21, and glyceraldehyde-3-phosphate dehydrogenase (GAPDH) from MBL (Nagoya, Japan), Cell Signaling Technology, Inc. (Beverly, MA), and Chemicon International, Inc. (Temecula, CA), respectively; rabbit polyclonal antibodies against cyclin-dependent kinase (CDK) 6 and E2F3 from Santa Cruz Biotechnology, Inc. (Santa Cruz, CA); goat polyclonal antibody against CDK4 from Santa Cruz Biotechnology, Inc.; enhanced Chemiluminescence plus detection reagent from GE Healthcare (Buckinghamshire, UK); Immobilon P membranes from Millipore Corp. (Bedford, MA); reagents for cDNA synthesis and real-time PCR from Toyobo (Osaka, Japan); a cell counting kit from Dojindo Laboratories (Kumamoto, Japan); and all other reagents from Sigma Chemical Co. or Wako Pure Chemical Co. (Osaka, Japan).

Cells

LX-2 cells were maintained in DMEM supplemented with 10% FBS (DMEM/FBS) and were plated at a density of 0.7–1.5 × 10^4 cells/cm^2 24 h prior to biological assay. Biological assays were done in DMEM/FBS unless stated otherwise. Mouse primary HSCs were isolated from male C57BL/6 mice by the pronase-collagenase digestion method as described previously (Uyama et al., 2006) and were cultured in DMEM/FBS.

Transient transfection of miRNA precursors and inhibitors

Precursor of miR-195, which was a double-strand RNA mimicking endogenous miR-195 precursor, and the negative control with a scrambled sequence were transfected into LX-2 cells using Lipofectamine 2000 (Invitrogen) at a final concentration of 50 nM in accordance with the manufacturer's instructions. Briefly, miRNA precursor and Lipofectamine 2000 were mixed at a ratio of 25 (pmol):1 (μl) in Opti-MEM I Reduced Medium (Invitrogen), incubated for 20 min at room temperature, and were then added to the cultures. After 24 h, the culture medium was replaced with fresh medium. Inhibitor of miR-195, which was designed to bind to endogenous miR-195 and inhibit its activity, and the negative control with a scrambled sequence were transfected similarly. After 6 h, the culture medium was changed and IFN-β was added successively.

Cell proliferation assay

LX-2 cells were plated at a density of 2 × 10^3 cells/well in 96-well plates 24 h prior to experiments. The culture medium was replaced by fresh medium containing different concentrations of IFNs at days 0 and 3. After 3, 5, and 7 days of treatment, cell proliferation was measured by WST-1 assay. In another experiment, the cells

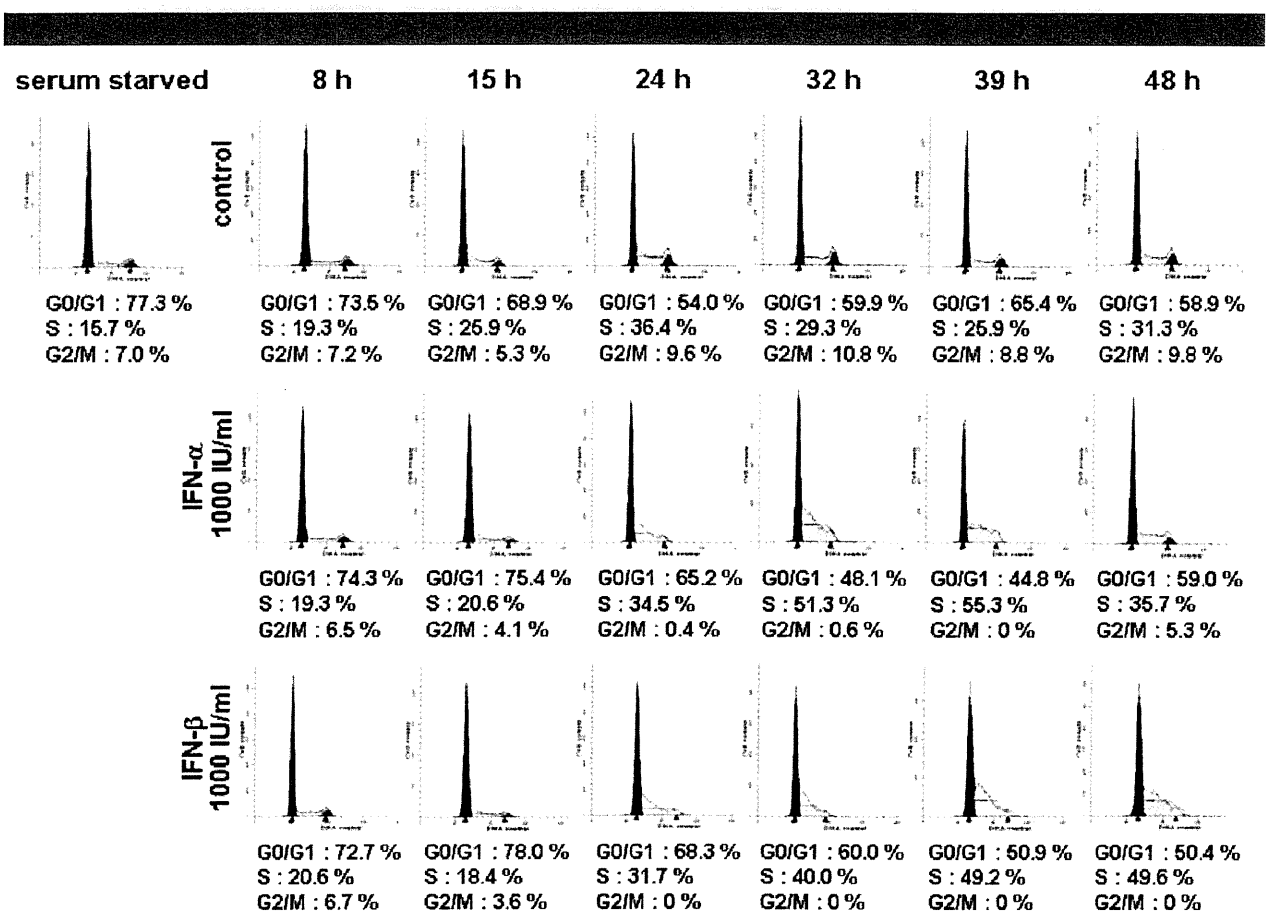

Fig. 2. Effect of IFN-α and -β on cell cycle distribution in human stellate cells. LX-2 cells synchronized in G0/G1 phase were then incubated with IFN-α or -β (1,000 IU/ml) in DMEM/FBS for the indicated periods. Control indicates non-treated cells. The cell cycle was analyzed by flow cytometry. The white, black, and shaded region indicates the histogram measured by flow cytometry, G0/G1 phase (left) or G2/M phase (right), and S phase, respectively, as analyzed by ModFIT LT software.

were plated at a density of 3×10^3 cells/well in 96-well plate for 24 h prior and were then transfected with the miR-195 precursor as described above. After 24 h, the medium was changed and the culture was continued for an additional 1–3 days before the measurement of cell proliferation.

Cell cycle analysis

Cells were serum starved for 24 h and then the medium was replaced with IFN-containing DMEM/FBS. At the indicated time points after treatment, the cells were harvested by trypsinization, washed in phosphate-buffered saline (PBS), and fixed in ice-cold 70% ethanol. The cells were washed in PBS and resuspended in PBS containing 500 μg/ml RNase A and incubated for 20 min. Cellular DNA was stained with propidium iodide at a final concentration of 25 μg/ml for 20 min. The cells were analyzed using a FACSCalibur HG flow cytometer (Becton Dickinson, Franklin Lakes, NJ). A total of 20,000 events were counted for each sample. Data were analyzed using ModFIT LT software (Verity Software House, Topsham, ME).

Quantitative real-time PCR

Quantitative real-time PCR was performed according to the method described elsewhere with use of a set of gene-specific oligonucleotide primers (Table 1) using an Applied Biosystems Prism 7500 (Applied Biosystems, Foster City, CA) (Ogawa et al., 2010). To detect miR-195 expression, the reverse transcription reaction was performed using a TaqMan microRNA Assay (Applied Biosystems) in accordance with the manufacturer's instructions. The expression level of GAPDH was used to normalize the relative abundance of mRNAs and miR-195.

Immunoblotting

Cells were lysed in RIPA buffer [50 mM Tris/HCl, pH 7.5, 150 mM NaCl, 1% NP-40, 0.5% sodium deoxycholate, 0.1% sodium dodecyl sulfate (SDS)] containing Protease Inhibitor Cocktail, Phosphatase Inhibitors Cocktail 1, and Phosphatase Inhibitor Cocktail 2 (Sigma). Proteins (20 μg) were electrophoresed in a 10% SDS–polyacrylamide gel and then transferred onto Immobilon P membranes (Ogawa et al., 2010). Immunoreactive bands were visualized by the enhanced chemiluminescence system using a Fujifilm Image Reader LAS-3000 (Fuji Medical Systems, Stamford, CT).

Luciferase reporter assay

Interaction of miR-195 to the 3′UTR of the cyclin E1 gene was tested according to the reported method (Ogawa et al., 2010). The 3′UTR of the cyclin E1 gene containing putative miR-195 target regions was obtained by PCR using cDNA derived from LX-2 and a primer set listed in Table 1. The obtained DNA fragments (497 bp) were inserted into a pmirGLO Vector (Promega, San Luis Obispo,

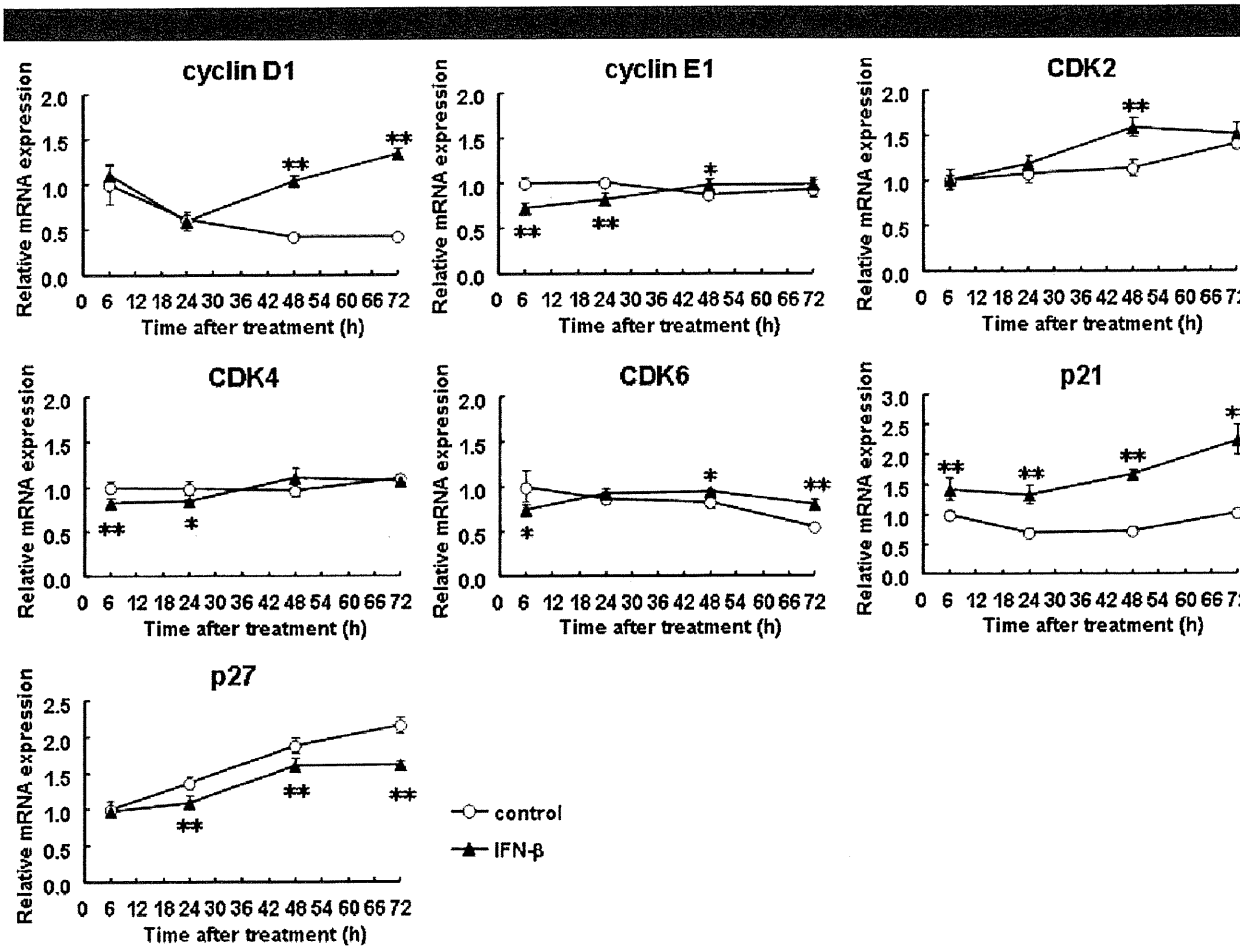

Fig. 3. Expression of cell cycle-related genes in stellate cells. LX-2 cells were incubated with IFN-β (1,000 IU/ml) for up to 72 h for determining the expression levels of mRNAs of cyclin D1, cyclin E1, CDK2, CDK4, CDK6, p21, and p27. Control indicates non-treated cells. *$P < 0.05$, **$P < 0.01$ compared with control.

CA). LX-2 cells, plated in 96-well plates at a density of 2×10^4 cells/well 24 h prior to experiment, were transfected with 200 ng of reporter plasmid and miRNA precursor using Lipofectamine 2000. After 24 h, the medium was changed to 20 μl of PBS. The Dual-Glo Luciferase Assay System (Promega) was used to analyze luciferase expression in accordance with the manufacturer's protocol. Firefly luciferase activity was normalized to *Renilla* luciferase activity to adjust for variations in transfection efficiency among experiments.

Statistical analysis

Data presented as graphs are the means ± SD of at least three independent experiments. Statistical analysis was performed using Student's *t*-test. $P < 0.05$ was considered significant.

Results

Reduction of miR-195 expression during activation of primary-cultured HSCs

It has been known that, when maintained in a plastic culture plate, freshly isolated primary-cultured HSCs undergo spontaneous activation and transformation into myofibroblastic cells that express α-SMA and produce fibrogenic mediators, such as type I collagen and transforming growth factor-β. In our preliminary experiments using primary-cultured mouse HSCs, we noticed that the cells drastically decreased the expression of miR-195 when they underwent spontaneous activation (unpublished observation). The present study confirmed this notion as shown in Figure 1A. miR-195 expression level certainly decreased in activation process of primary-cultured mouse HSCs. In contrast, the expression levels of α-SMA and cyclin E1 mRNA increased (Fig. 1B). Accordingly, we considered that miR-195 plays a role as an antiproliferative and antiactivating miRNA in HSCs. As a matter of fact, there was a study showing that miR-16 family including miR-195 inhibits proliferation of lung cancer cells by silencing cyclins D1 and E1, and CDK6 (Liu et al., 2008). The result indicated by Figure 1 and the cited study together drove us to explore the IFN's antiproliferative action on HSCs (Mallat et al., 1995; Shen et al., 2002), focusing on miR-195 and cell cycle-related genes.

Effects of IFN-α and -β on proliferation of HSCs

First, we investigated the effects of type I IFNs on the proliferation of LX-2 cells using a WST-1 assay. LX-2 cells in control culture continued to grow during the experimental

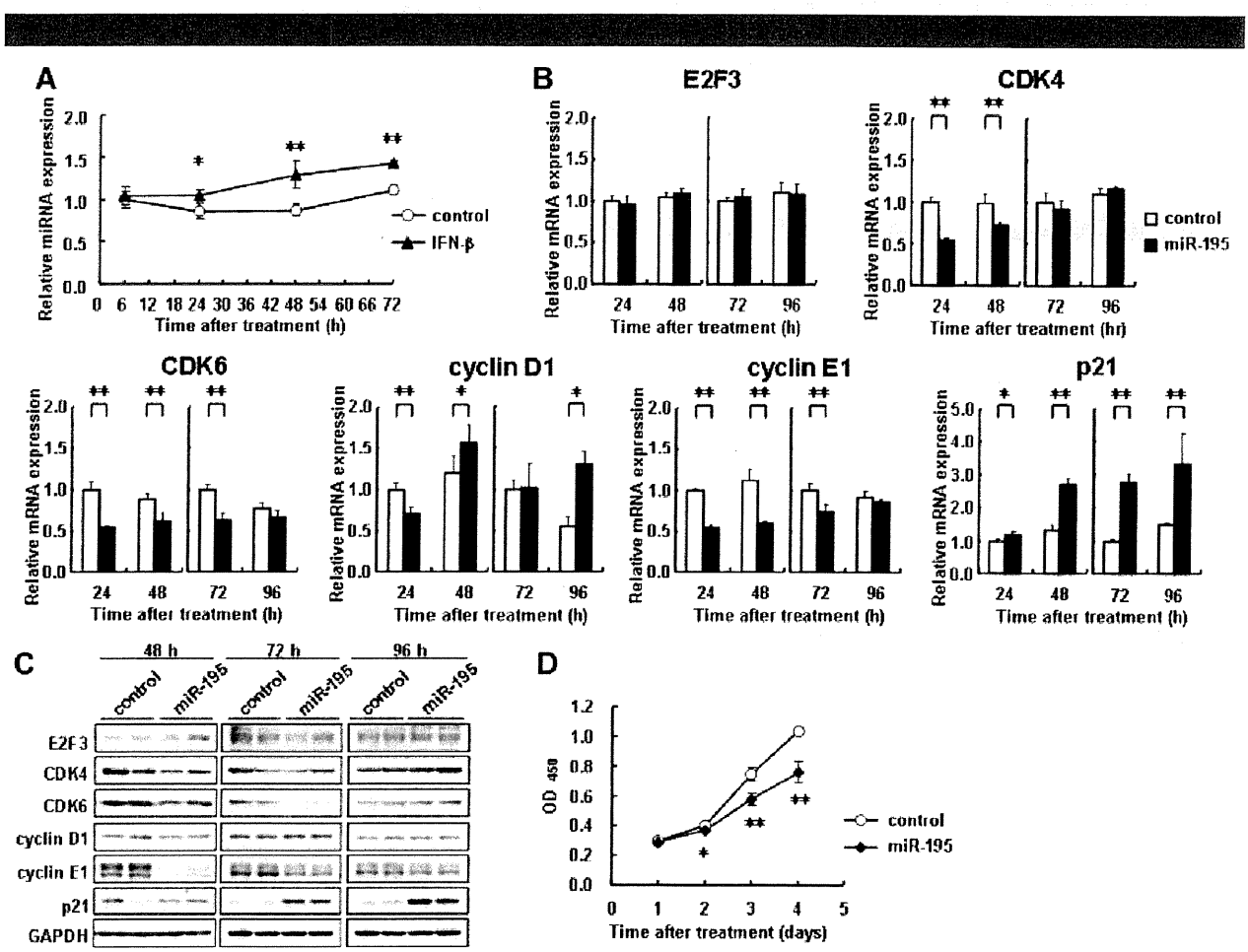

Fig. 4. Regulation of expression of cell cycle regulators by miR-195. A: LX-2 cells were incubated with IFN-β (1,000 IU/ml) for up to 72 h for determining the expression levels of miR-195. Control indicates non-treated cells. *$P < 0.05$, **$P < 0.01$ compared with control. B–D: LX-2 cells were transfected with 50 nM miR-195 precursor or a negative control (control). B: mRNA expression levels of E2F3, CDK4, CDK6, cyclin D1, cyclin E1, and p21 measured at 24, 48, 72, and 96 h post-transfection. C: Protein expression of E2F3, CDK4, CDK6, cyclin D1, cyclin E1, and p21 examined at 48, 72, and 96 h post-transfection. D: Growth of LX-2 cells transfected with 50 nM miR-195 precursor or a negative control (control) was measured using a WST-1 assay. *$P < 0.05$, **$P < 0.01$ compared with control.

period of 7 days (Fig. 1C). IFN-α and -β both, but the latter more actively, decreased cell proliferation time-dependently at a concentration of 1,000 IU/ml, supporting the previous studies (Mallat et al., 1995; Shen et al., 2002). Dose-dependency of the growth inhibition is shown in IFN concentrations from 10 to 1,000 IU/ml (Fig. 1D).

Effects of IFN-α and -β on cell cycle distribution

To elucidate the mechanism of the growth inhibitory effect of IFN, we next examined the change in cell cycle distribution in response to IFN-α and -β treatment by flow cytometry. LX-2 cells were synchronized in G0/G1 phase by serum starvation for 24 h. In non-treated cells (control), population in G0/G1 phase was reduced after serum exposure, which was accompanied by the increase of population in S phase. This cell cycle transition peaked at 24 h (Fig. 2, upper part). In cells treated with IFN-α or -β, the G0/G1 phase population was larger and the S phase population was smaller than in the control cells at 15 h and 24 h. In addition, the accumulation of cells in early S phase was observed at 32–48 h (Fig. 2, middle and lower parts). These delays in cell cycle shift were more potent in IFN-β-treated cells than in IFN-α-treated cells. It was concluded that type I IFN hampered HSC proliferation through a delay in the cell cycle at the transition from G1 to S phase and in the progression of S phase.

Regulation of cyclin E1 and p21 expression by IFN-β

IFN-β was chosen in the following experiments because of its more potent inhibition of cell cycle progression than IFN-α as described above. The transition from G1 to S phase and the progression of S phase are known to be influenced by various regulators (Golias et al., 2004). Among them, we found that IFN-β significantly decreased cyclin E1 mRNA expression levels by 0.6- to 0.7-fold at 6 and 24 h and increased p21 mRNA expression levels by 1.4- to 2.3-fold at 6, 24, 48, and 72 h in LX-2 cells (Fig. 3). The expression levels of CDK4 and CDK6 were also reduced by IFN-β at early phase with less extent. The others showed negligible change within 24 h although variable dynamics were seen thereafter; changes of cyclin D1, CDK2, and p27 expression at late phase were toward cell cycle promotion with currently unknown reason.

Regulation of miR-195 expression by IFN-β

The result indicated from Figure 1 strongly suggested the possibility that IFN-β increase the expression of miR-195 in LX-2 cells. To test this possibility, we examined the expression levels of miR-195 in IFN-β-treated LX-2 cells. As a result, the miR-195 expression level was significantly increased by IFN-β treatment at 24, 48, and 72 h (Fig. 4A).

Regulation of cyclin E1 and p21 expression by miR-195

The results obtained from experiments shown in Figures 3 and 4A led us to hypothesize that IFN-β up-regulates the expression of miR-195, which then down-regulates the expression of cyclin E1 and up-regulates the expression of p21. In addition, there had been a study reporting that miR-195 targets E2F3, CDK6, and cyclin D1 in addition to cyclin E1 (Xu et al., 2009). Under these considerations, we examined the changes in the expression levels of the above-mentioned cell cycle-related molecules and CDK4 by introducing miR-195

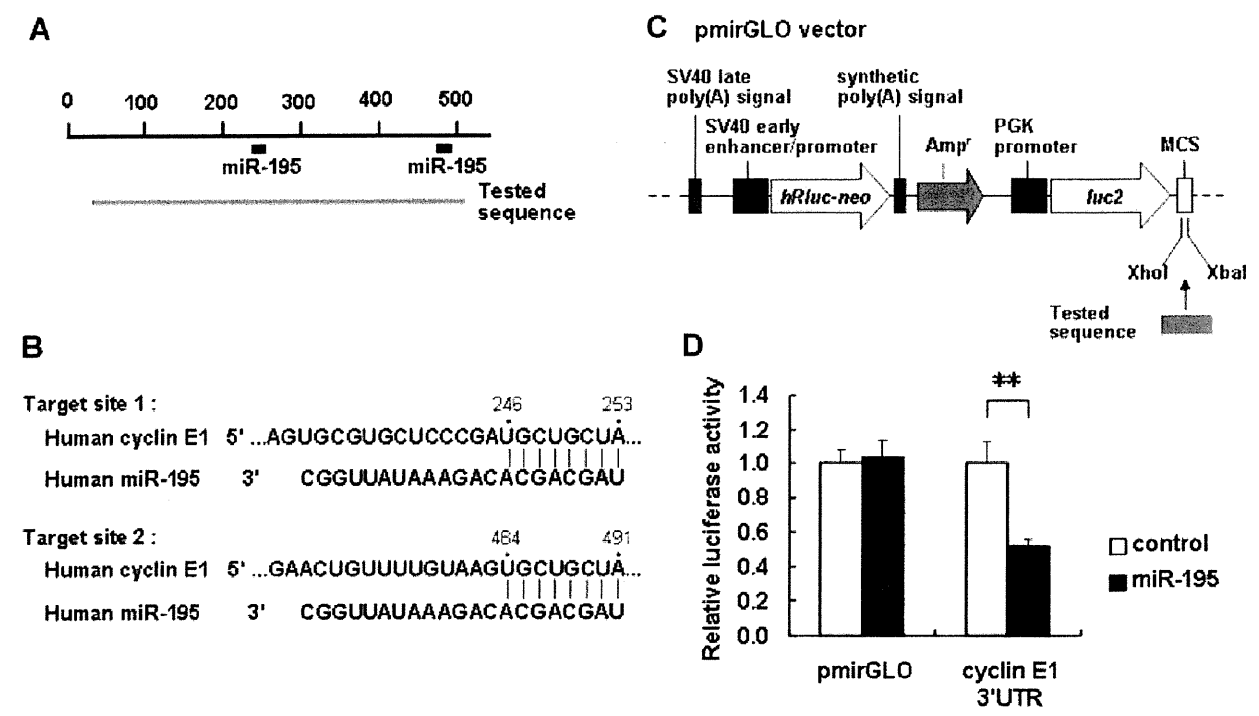

Fig. 5. Interaction of miR-195 with the 3′UTR of cyclin E1 mRNA. A: Schematic indication of the putative miR-195 target sites in the 3′UTR of the cyclin E1 mRNA. Tested sequences indicate the regions that were inserted into the luciferase reporter vector. B: Predicted pairing of the target region and miRNAs. C: Structure of the luciferase reporter vector (Ogawa et al., 2010). The putative miR-195 target region in cyclin E1 3′UTR (tested sequence) was ligated into the MCS. Arrows indicate the gene directions. Amp^R indicates an ampicillin resistance gene. D: Reporter gene assay of the interaction between the 3′UTR of cyclin E1 mRNA and miR-195 in LX-2 cells. Results are expressed as the relative activities against the activity in the presence of the control. $^*P < 0.05$, $^{**}P < 0.01$ compared with control.

precursor into LX-2 cells. Transfection of miR-195 precursor increased the miR-195 expression levels in LX-2 cells by up to 10,000–30,000 times compared with those in cells transfected with negative control (data not shown). Cyclin E1 mRNA and protein expression levels showed a remarkable reduction up to 72 h as result of miR-195 overexpression (Fig. 4B,C). On the other hand, p21 mRNA and protein expression levels showed a marked increase. CDK4, CDK6, and cyclin D1 expression levels were significantly changed at the mRNA level, but negligibly at the protein level. E2F3 mRNA and protein expression levels were unchanged (Fig. 4B,C). These results suggested that miR-195 mainly regulated cyclin E1 and p21 expression in LX-2 cells. Moreover, transfection of miR-195 precursor (50 nM) decreased the proliferation of LX-2 cells in the WST-1 assay (Fig. 4D). These results showed that miR-195 down-regulates endogenous cyclin E1 expression and up-regulates p21 expression, resulting in the attenuation of cell cycle progression and cell proliferation.

Interaction of miR-195 with cyclin E1 3′UTR in LX-2 cells

Next, we examined whether miR-195 interacted directly with cyclin E1 3′UTR in LX-2 cells. The predicted miRNA target sites for miR-195 in the cyclin E1 3′UTR were analyzed using TargetScan Human Release 5.1 (http://www.targetscan.org/). The cyclin E1 3′UTR contained two target sites for miR-195 (Fig. 5A,B). To investigate the direct interaction between them, the part of the cyclin E1 3′UTR containing the two miR-195 target sites (497 bp) was cloned from LX-2 cells, inserted the downstream of a firefly luciferase reporter gene in a pmirGLO vector (Fig. 5C), and cotransfected into LX-2 cells. As shown in Figure 5D, luciferase reporter activity decreased significantly in miR-195 precursor-transfected cells compared with cells transfected with a negative control of the precursor. These results suggested a direct interaction between miR-195 and cyclin E1 3′UTR in LX-2 cells. Binding site of miR-195 was not found in p21 3′UTR by TargetScan.

Regulation of cyclin E1 expression by IFN-β and miR-195

To confirm the contribution of miR-195 to the inhibitory effect of IFN-β on cyclin E1 expression, LX-2 cells were first transfected with 50 nM miR-195 inhibitor and then treated with 1,000 IU/ml IFN-β. As shown in Figure 6A, miR-195 inhibitor blocked the inhibitory effect of IFN-β on cyclin E1 mRNA expression at 16 and 24 h. Although there was no difference in the cyclin E1 mRNA expression between IFN-β-treated cells and non-treated cells (control) at 48 h, the cyclin E1 mRNA expression level in miR-195 inhibitor plus IFN-β-treated cells was up-regulated compared with non-treated cells (Fig. 6A). Immunoblot analysis revealed that miR-195 inhibitor elevated the cyclin E1 expression level of IFN-β-treated cells at 24 and 48 h (Fig. 6B).

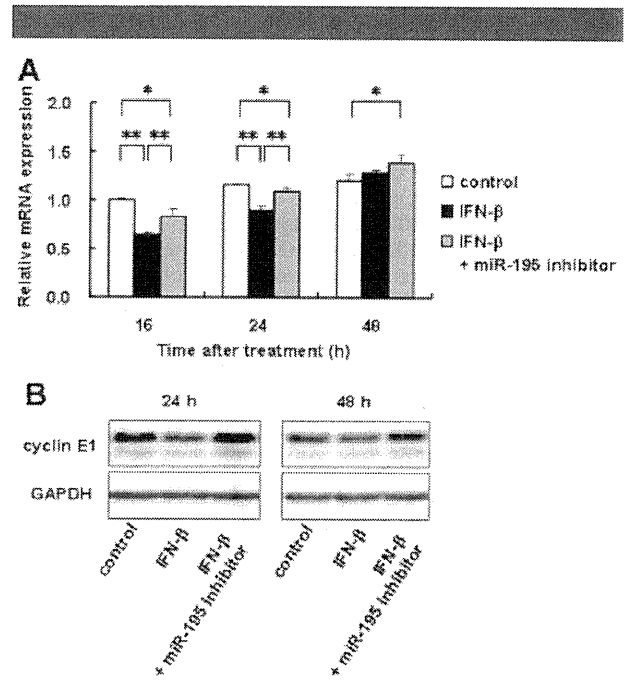

Fig. 6. Regulation of cyclin E1 expression by IFN-β and miR-195. LX-2 cells were transfected with 50 nM miR-195 inhibitor or a negative control. After 6 h, the culture medium was changed and then IFN-β (1,000 IU/ml) was added. Cells were then incubated for the indicated time periods. A: mRNA expression levels of cyclin E1. B: Protein expression levels of cyclin E1. GAPDH are for loading adjustment. Control; cells were transfected with a negative control and incubated without IFN-β. *$P < 0.05$, **$P < 0.01$.

Discussion

In this study, we showed that IFN-β is more antiproliferative on LX-2 cells than IFN-α, which appears to be contradictory to their known mechanism of action: both IFN-α and -β exert their activities through the common signaling pathway, beginning with binding to the same type I IFN receptor (IFNAR) consisting of IFNAR1 and IFNAR2, which activate the common components of janus kinase/signal transducer and activator of transcription (STAT) pathway (Darnell et al., 1994). However, a similar activity difference between the IFNs has also been demonstrated in colon cancer cell lines (Katayama et al., 2007) and in rat HSCs (Shen et al., 2002). Some studies showed that IFN-β but not IFN-α formed a stable complex with IFNARs, suggesting that IFN-β may interact with IFNAR chains in a manner different from IFN-α (Croze et al., 1996; Russell-Harde et al., 1999).

We showed here that IFN-β down-regulated the expression of cyclin E1 and up-regulated the expression of p21, which caused the cells to be less active proceeding in the transition from G0 to G1 phase and in the progression of S phase. The cell cycle is regulated by various molecules, such as cyclins and CDKs. Cyclin E is essential in activating CDK2. The cyclin E-CDK2 complex phosphorylates pRb at G1 phase, leading to gene transcription activities that are needed in S phase, and also activates the factors involved in DNA replication at early S phase (Golias et al., 2004). It has been reported that cyclin E1 expression increased in non-parenchymal cells of human fibrotic liver and that cyclin E1-deficient mice developed milder liver fibrosis compared with wild-type mice after CCl_4 administration (Nevzorova et al., 2010). These results imply that cyclin E1 regulates the progression of liver fibrosis by accelerating HSC proliferation.

The most frequent miRNAs that targets cyclin E1 are the miR-16 family, which consists of miR-15, -16, -195, -424, and -497 (Liu et al., 2008; Wang et al., 2009). We here observed the induction of miR-195 by IFN-β. miR-195 was reported to be down-regulated in human HCC tissues and to suppress HCC growth through the targeted interference of cyclin D1, CDK6, and E2F3 in a *xenograft* mouse model (Xu et al., 2009), while it was reported to target cyclin E1 in addition to the above-mentioned factors in A549 cells (Liu et al., 2008). miR-15b and miR-16 are down-regulated concomitantly with HSC activation and their overexpression induces apoptosis and a delay of cell cycle in HSCs by targeting Bcl-2 and cyclin D1 (Guo et al., 2009a,b). However, the role of miR-195 in HSCs remains unknown. We showed here that miR-195 expression was

decreased during spontaneous activation of primary-cultured mouse HSCs and that miR-195 interacted with cyclin E1 3′UTR and lowered the expression levels of the cyclin E1 mRNA and protein in LX-2 cells. These results suggest that the down-regulation of miR-195 may associate with the proliferation of HSCs in fibrotic liver similarly to miR-15 and miR-16. In this study, the changes of the protein expression levels of E2F3, CDK6, and cyclin D1, which were reported to be regulated by miR-195 (Xu et al., 2009), were negligible by miR-195, although the exact reason for this phenomenon was not determined. However, because the total context scores obtained by TargetScan were −0.73 for cyclin E1, −0.33 for E2F3, −0.32 for cyclin D1, and −0.09 for CDK6, the result obtained here was thought to be reasonable. In addition, minimal or negligible effect of miR-195 on the expression of E2F3, CDK4, CDK6, and cyclin D1 was compatible with that of IFN-β on these factors. Furthermore, inhibition of miR-195 by miR-195 inhibitor attenuated the effect of IFN-β on cyclin E1 expression, though not so strong. Taken together, it is most likely that the down-regulation of cyclin E1 by IFN-β treatment in HSCs is mediated through miR-195 up-regulation. The mechanism through which IFN-β induces miR-195 in LX-2 cells need to be explored further.

It is well known that IFNs induce the expression of p21 in various cancer cells (Sangfelt et al., 1999; Katayama et al., 2007). We also observed the up-regulation of p21 in IFN-β-treated cells. Therefore, p21, in addition to cyclin E1, may play a role in IFN-induced growth inhibition of HSCs. Until now, it has been reported that IFNs induce p21 expression through the binding of STAT and IFN regulatory factor, which are critical signaling molecules after IFN-IFNAR interaction, to p21 gene promoter (Gartel and Tyner, 1999). Unexpectedly, we found the up-regulation of p21 by miR-195 (Fig. 4). The results obtained here raise a new possibility that the up-regulation of p21 by IFN-β in HSCs may be partially mediated through miR-195.

In conclusion, type I IFN, in particular IFN-β, inhibited the proliferation of human HSCs by delaying the cell cycle in G1 to early S phase through the down-regulation of cyclin E1 and up-regulation of p21. The cyclin E1 down-regulation and p21 up-regulation were partially mediated by miR-195 that was up-regulated by IFN-β. This study raises a new mechanistic aspect of the antifibrotic effect of IFN in liver fibrosis and the possibility of influencing miR-195 as a therapeutic strategy for liver fibrosis.

Acknowledgments

This work was supported by a grant from the Ministry of Health, Labour and Welfare of Japan to N. Kawada (2008–2010).

Literature Cited

Bartel DP. 2004. MicroRNAs: Genomics, biogenesis, mechanism, and function. Cell 116:281–297.

Bataller R, Brenner DA. 2001. Hepatic stellate cells as a target for the treatment of liver fibrosis. Semin Liv Dis 21:437–451.

Chang XM, Chang Y, Jia A. 2005. Effects of interferon-alpha on expression of hepatic stellate cell and transforming growth factor-beta1 and alpha-smooth muscle actin in rats with hepatic fibrosis. World J Gastroenterol 11:2634–2636.

Croze E, Russell-Harde D, Wagner TC, Pu H, Pfeffer LM, Perez HD. 1996. The human type I interferon receptor. Identification of the interferon beta-specific receptor-associated phosphoprotein. J Biol Chem 271:33165–33168.

Darnell JE, Kerr IM, Stark GR. 1994. Jak-STAT pathways and transcriptional activation in response to IFNs and other extracellular signaling proteins. Science 264:1415–1421.

Fort J, Pilette C, Veal N, Oberti F, Gallois Y, Douay O, Rosenbaum J, Cales P. 1998. Effects of long-term administration of interferon alpha in two models of liver fibrosis in rats. J Hepatol 29:263–270.

Friedman SL. 2000. Molecular regulation of hepatic fibrosis, an integrated cellular response to tissue injury. J Biol Chem 275:2247–2250.

Gartel AL, Tyner AL. 1999. Transcriptional regulation of the p21(WAF1/CIP1) gene. Exp Cell Res 246:280–289.

Golias CH, Charalabopoulos A, Charalabopoulos K. 2004. Cell proliferation and cell cycle control: A mini review. Int J Clin Pract 58:1134–1141.

Guo CJ, Pan Q, Jiang B, Chen GY, Li DG. 2009a. Effects of upregulated expression of microRNA-16 on biological properties of culture-activated hepatic stellate cells. Apoptosis 14:1331–1340.

Guo CJ, Pan Q, Li DG, Sun H, Liu BW. 2009b. miR-15b and miR-16 are implicated in activation of the rat hepatic stellate cell: An essential role for apoptosis. J Hepatol 50:766–778.

Inagaki Y, Nemoto T, Kushida M, Meng Y, Higashi K, Ikeda K, Kawada N, Shirasaki F, Takehara K, Sugiyama K, Fujii M, Yamauchi H, Nakao A, de Crombrugghe B, Watanabe T, Okazaki I. 2003. Interferon alpha down-regulates collagen gene transcription and suppresses experimental hepatic fibrosis in mice. Hepatology 38:890–899.

Ji JF, Shi J, Budhu A, Yu ZP, Forgues M, Roessler S, Ambs S, Chen YD, Meltzer PS, Croce CM, Qin LX, Man K, Lo CM, Lee J, Ng IOL, Fan J, Tang ZY, Sun HC, Wang XW. 2009a. MicroRNA expression, survival, and response to interferon in liver cancer. N Engl J Med 361:1437–1447.

Ji JL, Zhang JS, Huang GC, Qian J, Wang XQ, Mei S. 2009b. Over-expressed microRNA-27a and 27b influence fat accumulation and cell proliferation during rat hepatic stellate cell activation. FEBS Lett 583:759–766.

Katayama T, Nakanishi K, Nishihara H, Kamiyama N, Nakagawa T, Kamiyama T, Iseki K, Tanaka S, Todo S. 2007. Type I interferon prolongs cell cycle progression via p21(WAF1/CIP1) induction in human colon cancer cells. Int J Oncol 31:613–620.

Liu Q, Fu HJ, Sun F, Zhang HM, Tie Y, Zhu J, Xing RY, Sun ZX, Zheng XF. 2008. miR-16 family induces cell cycle arrest by regulating multiple cell cycle genes. Nucleic Acids Res 36:5391–5404.

Mallat A, Preaux AM, Blazejewski S, Rosenbaum J, Dhumeaux D, Mavier P. 1995. Interferon alpha and gamma inhibit proliferation and collagen synthesis of human Ito cells in culture. Hepatology 21:1003–1010.

Nevzorova YA, Bangen JM, Gassler N, Haas U, Weiskirchen R, Tacke F, Sicinski P, Trautwein C, Liedtke C. 2010. Cyclin E1 controls the cell cycle activity of hepatic stellate cells and triggers fibrogenesis in mice. J Hepatol 52:S374–S375.

Ogawa T, Kawada N, Ikeda K. 2009. Effect of natural interferon alpha on proliferation and apoptosis of hepatic stellate cells. Hepatol Int 3:497–503.

Ogawa T, Iizuka M, Sekiya Y, Yoshizato K, Ikeda K, Kawada N. 2010. Suppression of type I collagen production by microRNA-29b in cultured human stellate cells. Biochem Biophys Res Commun 391:316–321.

Pedersen IM, Cheng G, Wieland S, Volinia S, Croce CM, Chisari FV, David M. 2007. Interferon modulation of cellular microRNAs as an antiviral mechanism. Nature 449:919–922.

Pestka S, Langer JA, Zoon KC, Samuel CE. 1987. Interferons and their actions. Annu Rev Biochem 56:727–777.

Russell-Harde D, Wagner TC, Perez HD, Croze E. 1999. Formation of a uniquely stable type I interferon receptor complex by interferon beta is dependent upon particular interactions between interferon beta and its receptor and independent of tyrosine phosphorylation. Biochem Biophys Res Commun 255:539–544.

Sangfelt O, Erickson S, Castro J, Heiden T, Gustafsson A, Einhorn S, Grander D. 1999. Molecular mechanisms underlying interferon-alpha-induced G0/G1 arrest: CKI-mediated regulation of G1 Cdk-complexes and activation of pocket proteins. Oncogene 18:2798–2810.

Shen H, Zhang M, Minuk GY, Gong YW. 2002. Different effects of rat interferon alpha, beta and gamma on rat hepatic stellate cell proliferation and activation. BMC Cell Biol 3:9.

Tanabe J, Izawa A, Takemi N, Miyauchi Y, Torii Y, Tsuchiyama H, Suzuki T, Sone S, Ando K. 2007. Interferon-beta reduces the mouse liver fibrosis induced by repeated administration of concanavalin A via the direct and indirect effects. Immunology 122:562–570.

Uyama N, Zhao L, Van Rossen E, Hirako Y, Reynaert H, Adams DH, Xue Z, Li Z, Robson R, Pekny M, Geerts A. 2006. Hepatic stellate cells express synemin, a protein bridging intermediate filaments to focal adhesions. Gut 55:1276–1289.

Uze G, Schreiber G, Piehler J, Pellegrini S. 2007. The receptor of the type I interferon family. Curr Top Microbiol Immunol 316:71–95.

Venugopal SK, Jiang J, Kim TH, Li Y, Wang SS, Torok NJ, Wu J, Zern MA. 2010. Liver fibrosis causes downregulation of miRNA-150 and miRNA-194 in hepatic stellate cells, and their overexpression causes decreased stellate cell activation. Am J Physiol Gastrointest Liver Physiol 298:G101–G106.

Wang F, Fu XD, Zhou Y, Zhang Y. 2009. Down-regulation of the cyclin E1 oncogene expression by microRNA-16-1 induces cell cycle arrest in human cancer cells. BMB Rep 42:725–730.

Xu L, Hui AY, Albanis E, Arthur MJ, O'Byrne SM, Blaner WS, Mukherjee P, Friedman SL, Eng FJ. 2005. Human hepatic stellate cell lines, LX-1 and LX-2: New tools for analysis of hepatic fibrosis. Gut 54:142–151.

Xu T, Zhu Y, Xiong YJ, Ge YY, Yun JP, Zhuang SM. 2009. MicroRNA-195 suppresses tumorigenicity and regulates G(1)/S transition of human hepatocellular carcinoma cells. Hepatology 50:113–121.

The American Journal of Pathology, Vol. 179, No. 2, August 2011

DOI: 10.1016/j.ajpath.2011.05.006

Tumorigenesis and Neoplastic Progression

Promotion of Liver and Lung Tumorigenesis in DEN-Treated Cytoglobin-Deficient Mice

Le Thi Thanh Thuy,*† Takashi Morita,‡ Kayo Yoshida,‡ Kenichi Wakasa,§ Masashi Iizuka,*† Tomohiro Ogawa,*† Mami Mori,* Yumiko Sekiya,*† Shinobu Momen,*† Hiroyuki Motoyama,* Kazuo Ikeda,¶ Katsutoshi Yoshizato,*†‖ and Norifumi Kawada*†

From the Departments of Hepatology, Molecular Genetics,‡ and Diagnostic Pathology,§ and the Liver Research Center,† Graduate School of Medicine, Osaka City University, Osaka; the Department of Anatomy and Cell Biology,¶ Graduate School of Medical Sciences, Nagoya City University, Aichi; and the Academic Advisor's Office,‖ PhoenixBio Co., Ltd., Hiroshima, Japan*

Cytoglobin (Cygb) is a recently discovered vertebrate globin with molecular characteristics that are similar to myoglobin. To study the biological function of Cygb *in vivo*, we generated *Cygb* knockout mice and investigated their susceptibility to *N*,*N*-diethylnitrosamine (DEN)–induced tumorigenesis. Four-week-old male mice were administered DEN in drinking water at a dose of 25 ppm for 25 weeks or 0.05 ppm for 36 weeks. *Cygb* deficiency promoted the DEN-induced development of liver and lung tumors. All $Cygb^{+/-}$ and $Cygb^{-/-}$ mice treated with 25-ppm DEN exhibited liver tumors, compared with 44.4% of their wild-type counterparts. Lung tumors were present only in *Cygb*-deficient mice. More than 40% of $Cygb^{-/-}$ mice developed liver and lung tumors at the nontoxic dose of DEN (0.05 ppm), which did not induce tumors in wild-type mice. *Cygb* loss was associated with increased cancer cell proliferation, elevated extracellular signal–regulated kinase and Akt activation, overexpression of IL-1β, IL-6, Tnfα, and Tgfβ3 mRNAs, and hepatic collagen accumulation. *Cygb*-deficient mice also exhibited increased nitrotyrosine formation and dysregulated expression of cancer-related genes (cyclin D2, p53, Pak1, Src, Cdkn2a, and Cebpa). These results suggest that *Cygb* deficiency induces susceptibility to cancer development in the liver and lungs of mice exposed to DEN. Thus, globins such as Cygb will shed new light on the biological features of organ carcinogenesis. *(Am J Pathol 2011, 179:1050–1060; DOI: 10.1016/j.ajpath.2011.05.006)*

Cytoglobin (Cygb) was originally identified in 2001 as a protein up-regulated in rat hepatic stellate cells under profibrotic conditions. Accordingly, Cygb was originally termed a stellate cell activation-associated protein[1] until it was identified as the fourth globin in mammals.[2,3] Human Cygb displays approximately 25% amino acid identity with vertebrate myoglobin and hemoglobin and 16% identity with human neuroglobin. The *Cygb* gene is localized to chromosome 17q25.3 in humans and chromosome 11E2 in mice.

Unlike myoglobin, which is tissue restricted to cardiomyocytes and skeletal myofibers, hemoglobin in erythrocytes, and neuroglobin in the nervous system, Cygb is ubiquitously expressed in the cytoplasm of mesenchymal fibroblastic cells in many organs, including the heart, lung, liver, kidneys, small intestine, and spleen. The presence of Cygb in the nucleus of these cells has also been reported.[4,5] In particular, Cygb was present in stellate cells and myofibroblasts in the liver and pancreas, reticulocytes in the spleen, mesenchymal cells in the submucosal layer of the gut, and the mesangium and stromal cells of the kidney.[4] An interesting aspect of Cygb expression is its presence in visceral cells, with a strong storage ability for vitamin A. Thus, Cygb may facilitate the diffusion of oxygen through tissues, scavenge nitric oxide (NO) or other reactive oxygen species, or serve a protective function during oxidative stress.[6] However, the precise physiological role of Cygb *in vivo* remains unresolved. Cygb is considered a hypoxia-responsive molecule because its mRNA expression is augmented under hypoxia in fibroblastic cell lineages and rat brain.[7] Hypoxia-inducible factor 1 is assumed to be an important transcription factor for *Cygb* because hypoxia-responsive elements at positions -141, -144, and -448 are essential for the acti-

Supported by a Grant-in-Aid for Scientific Research from the Japan Society for the Promotion of Science [grant 21390232 (2009) to N.K.]; grants from the Ministry of Health, Labour, and Welfare of Japan (2008); and the Thrust Area Research grant from Osaka City University (2008).

Accepted for publication May 2, 2011.

Presented in part at the 16th International Symposium on Cells of the Hepatic Sinusoid, Pasadena, CA, September 2, 2010.

Address reprint requests to Norifumi Kawada, M.D., Ph.D., Department of Hepatology, Graduate School of Medicine, Osaka City University, 1-4-3 Asahimachi, Abeno, Osaka 545-8585, Japan. E-mail: kawadanori@med.osaka-cu.ac.jp.

vation of CYGB gene expression, and the binding of hypoxia-inducible factor 1 to this area has been confirmed.[8,9] In contrast, CYGB overexpression rescues the human neuronal cell line TE671 from prooxidant Ro19-8022–induced DNA damage.[10] CYGB overexpression also protected human neuroblastoma SH-SY5Y cells from H_2O_2-induced cell death.[11,12] Furthermore, the *in vitro* and *in vivo* overexpression of Cygb in rat hepatic stellate cells protected these cells against oxidative stress and inhibited their differentiation into an active phenotype.[13] Together, these reports suggest that Cygb may act as a cytoprotective and radical-scavenging molecule in addition to its function as a gas carrier.

Although the function of Cygb *in vivo* remains largely unknown, down-regulation of CYGB has been reported in several human cancerous tissues and human cancer cell lines. Decreased expression of CYGB and the hypermethylation of the CYGB promoter has been reported in patients with tylosis, non–small-cell lung carcinoma tissues, head and neck cancers, ovarian cancers, and breast cancers.[14–18] McRonald et al[14] reported that CYGB gene expression in tylosis with esophagus cancer was reduced to approximately 70% compared with the normal esophagus and was accompanied by hypermethylation of the promoter. Xinarianos et al[15] reported a significant reduction of CYGB mRNA expression in non-small-cell lung carcinoma tissues and hypermethylation of CYGB, compared with healthy samples. Similar results were reported in head and neck, ovarian, and breast cancer tissues.[16–18] In addition, Shivapurkar et al[19] reported high levels of CYGB promoter methylation in lung, breast, bladder, and colon cancers and in leukemia in humans. The augmented growth of NCI-H661 lung cancer cells that were CYGB silenced by RNA interference and the suppression of NCI-H228 cell proliferation in cells stably transfected with plasmids containing CYGB cDNA have also been reported.[19] These reports indicate a tumor suppressor function of *Cygb*.

To study the biological function of *Cygb* at the tissue level, we first generated *Cygb*-deficient ($Cygb^{-/-}$) mice and observed that, after treatment with *N,N*-diethylnitrosamine (DEN), $Cygb^{-/-}$ mice showed a high incidence of tumor development in the liver and lungs. These results indicate the tumor suppressor role of *Cygb in vivo*.

Materials and Methods

Materials

All experimental reagents were obtained from Sigma Chemical Co (St. Louis, MO) or Wako Pure Chemical Co (Osaka, Japan), unless otherwise stated.

Construction of the Targeting Vector

Mice lacking exon 1 of the *Cygb* gene were generated using the lox-P system, as previously described.[20] The targeting vector (pTVneo/*Cygb*) was constructed from PCR DNA fragments from 129Sv mouse genomic DNA. Two DNA fragments were used as the 3′ and 5′ arms. One fragment contained *Cygb* exons 2, 3, and 4 (6.5 kb); and the other contained the transcription initiation site in exon 1 and the 5′ upstream sequence of the *Cygb* gene (6.0 kb). The neomycin-resistance gene, driven by the phosphoglycerate kinase 1 promoter, flanking the lox-P sequences was inserted into the arms (Figure 1A).

Embryonic stem cells (1×10^7 cells/mL) were transfected with a linearized targeting vector (20 μg) by electroporation and cultured in selection medium containing 150 μg/mL geneticine (G418). Of 480 neomycin-resistant clones, 6 (1.2%) were homologous recombinants by Southern blotting using the 5′ probe (data not shown).

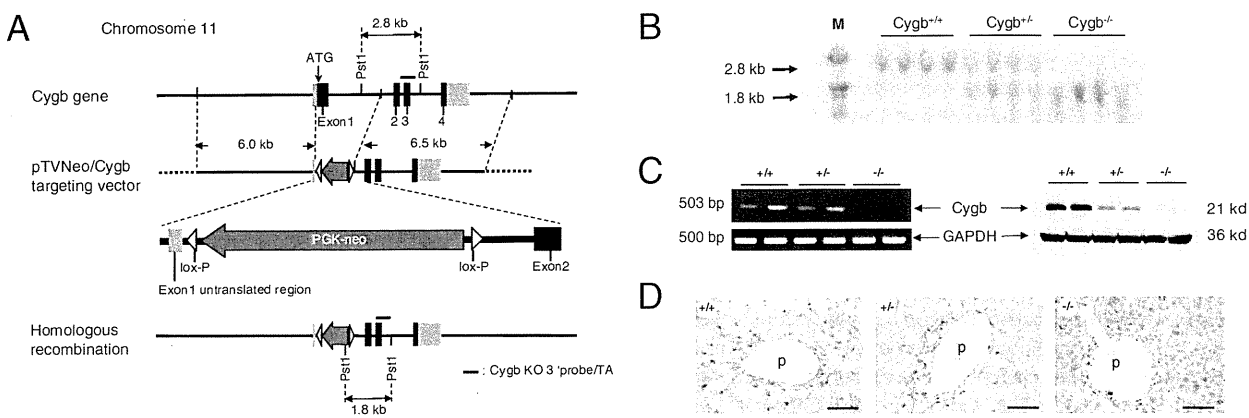

Figure 1. Generation of *Cygb*-deficient mice. **A:** Strategy for inactivation of the *Cygb* gene by homologous recombination in embryonic stem cells. A partial genomic map of the *Cygb* gene with coding exons (**black boxes**), noncoding regions (**light gray boxes**), and flanking introns (**solid lines**) is shown (**top**). Targeting vector pTVneo/*Cygb* with homology to the *Cygb* gene locus is shown (**middle**). The translation initiation site in exon 1 was replaced with a neomycin-resistance cassette. The predicted *Cygb* gene locus after homologous recombination is shown (**bottom**). **B:** Southern blot analysis shows the sizes of the wild-type (2.8-kb) and disrupted (1.8-kb) *Cygb* fragments after PstI cleavage. M, molecular weight marker. **C:** RT-PCR and immunoblot analysis of Cygb expression in the liver from $Cygb^{+/+}$, $Cygb^{+/-}$, and $Cygb^{-/-}$ mice. GAPDH was used as a loading control. **D:** Representative IHC images of Cygb in the liver of $Cygb^{+/+}$, $Cygb^{+/-}$, and $Cygb^{-/-}$ mice. Cygb is present along the sinusoids of $Cygb^{+/+}$ mice, whereas it is undetectable in $Cygb^{-/-}$ mice. p, portal vein. Scale bar = 50 μm.

Production of Cygb-*Deficient Mice*

Two clones were aggregated with C57BL/6-DBA2 F1 mouse morulae, and one produced chimeric mice that transmitted the knockout (KO) construct. Chimeric males were mated with C57BL/6J females to obtain *Cygb* heterozygous mice that were backcrossed to the C57BL/6J background for more than nine generations. To assess the role of the *Cygb* gene in development, we intercrossed *Cygb* heterozygous mice. The litter sizes were normal, and analysis of the tail biopsy specimens at the age of 4 weeks, from 102 offspring from heterozygote crosses, revealed the presence of homozygous mutant mice at a frequency of 24%. The homozygotes appeared normal morphologically and histopathologically 1 month after birth. Four-week-old $Cygb^{+/+}$ (wild-type), $Cygb^{+/-}$ (heterozygote), and $Cygb^{-/-}$ (homozygote) male mice were used in this study.

All mice were cared for according to the guidelines approved by the Institutional Animal Care and Use Committee of Osaka City University, Osaka.

Genotyping of Mice

PCR genotyping of mouse tail DNA produced the expected 338-bp product from wild-type mice using the following primer pairs: forward, 5′-CTCCCAGCCGGGACCGCG-GTGGCCTT-3′; and reverse, 5′-GGAGCCGAGGCCGGT-GCGTGCGAGGC-3′. A 529-bp product was diagnostic for the *Cygb* KO allele using the described forward primer and the following reverse primer: 5′-GTGGGGTGGGATT-AGATAAATGCCTGCTCT-3′. PCR was performed in a 15-μL reaction mixture containing 1 μL of extract from mouse tail DNA, which was digestion extracted using LYPPO (Gene Modification R&D Co Ltd, Osaka), according to the manufacturer's protocol; 1 μmol/L of each primer; 2.5% to 5% dimethyl sulfoxide; and 0.5 U GO Taq polymerase (Promega, San Luis Obispo, CA). PCRs were performed for 40 cycles, each cycle being 1 minute at 94°C, 30 seconds at 70°C, and 1 minute at 72°C.

Southern blot analysis confirmed the *Cygb*-null allele. Genomic tail DNA (5 μg) was cleaved with PstI, subjected to agarose gel electrophoresis, blotted onto nylon membranes, and hybridized to the ^{32}P-labeled *Cygb* KO 3′ probe/TA (Figure 1A). DNA fragments of 2.8 and 1.8 kb represented the *Cygb* wild-type and null alleles, respectively.

RT-PCR was performed to confirm the absence of Cygb mRNA in tissues. Total RNA was extracted from the homogenates of liver tissues using the RNeasy Mini Kit (Qiagen, Valencia, CA). cDNA was synthesized using 1 μg of total RNA, ReverTra Ace (Toyobo, Osaka), and oligo $(dT)_{12-18}$ primers, according to the manufacturer's instructions. Thirty-five PCR cycles (30 seconds at 94°C, 30 seconds at 68°C, and 1 minute at 72°C) were run using the following mouse Cygb primers: forward, 5′-GCGACATGGAGATAGAGCGT-3′; and reverse, 5′-CTG-TACCCAGCCCACTTCCT-3′. This generated a 503-bp product and glyceraldehyde-3-phosphate dehydrogenase (GAPDH) primers: forward, 5′-CGCCTGGTCAC-CAGG-3′; and reverse, 5′-CAGTTGGTGGTGCAGGA-3′). A 500-bp product was generated.

Administration of DEN

DEN (0.95 g/mL) was obtained from Sigma Chemical Co. A stock solution of DEN was prepared by dissolving 1 g (1.06 mL) of DEN in 400 mL of water. The stock solution was diluted 100-fold before use to obtain a final concentration of 25-mg DEN per 1000-mL water (25 ppm) for the high-dose experiment. The 25-ppm solution was further diluted 500-fold to obtain a final concentration of 0.05-mg DEN per 1000-mL water (0.05 ppm) for the low-dose experiment. The diluted solution (25 or 0.05 ppm) was placed in a shaded serving bottle and administered to the animals instead of water. The diluted solution was prepared weekly. The administration of DEN to male mice began at the age of 4 weeks for 25 weeks in the high-dose experiment (25 ppm) and for 36 weeks in the low-dose experiment (0.05 ppm). Each experiment contained three groups ($Cygb^{+/+}$, $Cygb^{+/-}$, and $Cygb^{-/-}$) with a

Table 1. Primary Antibodies Used for IHC Analyses

Antigen*	Source	Name/clone; catalog no.	Incubation
AFP	US Biological, Swampscott, MA	F4100-16A (Go)	Overnight 4°C, 1:20
CK19	Santa Cruz Biotechnology, Santa Cruz, CA	Polyclonal (Rb); sc-33111	Overnight 4°C, 1:100
CRBP-1	Santa Cruz Biotechnology	Polyclonal (Rb); sc-30106	Overnight 4°C, 1:100
Cygb	Our laboratory†	Polyclonal (Rb)	Overnight 4°C, 1:100
Erk	Cell Signaling, Danvers, MA	Monoclonal (Rb); 4695	Overnight 4°C, 1:300
PCNA	Dako, Glostrup, Denmark	Monoclonal (Mo)‡; clone: PC-10	Overnight 4°C, 1:200
Phosphorylated Erk	Cell Signaling	Monoclonal (Rb); 4370	Overnight 4°C, 1:200
α-SMA	Dako	Monoclonal (Mo)‡; clone: 1A4	30 minutes at room temperature, 1:100
Desmin	Santa Cruz Biotechnology	Polyclonal (Go); sc-7559	Overnight 4°C, 1:100

*All antigens were retrieved by autoclaving for 15 minutes in 0.01 mol/L citrate buffer containing 0.05% Tween 20 (pH 6.0), except for desmin, which was used in Tris-EDTA buffer (pH 9.0).

†Data taken from Kawada et al.[1]

‡For mouse primary antibodies, after antigen retrieval, sections were incubated with goat anti-mouse IgG Fab fragments (Jackson ImmunoResearch Laboratories) for 1 hour at room temperature (1:100) to block nonspecific background staining.

AFP, alpha-fetoprotein.

minimum of seven mice per group. Mice were sacrificed after the completion of DEN treatment.

Necropsy

At necropsy, mice were weighed, anesthetized, and examined for grossly visible lesions in whole organs. Livers and lungs were excised, weighed (in the case of liver), and examined for macroscopic lesions. The number of macroscopic abnormal masses ≥1 mm was determined in addition to the size of the mass by taking the average of the largest and smallest length of the mass. For histological examination, 2- to 3-mm-thick sections from nontumor or tumor tissues were fixed in 10% formalin for 24 hours and embedded in paraffin. The samples were then sectioned at 5 μm and stained with H&E.

IHC and TUNEL Assays

For immunohistochemistry (IHC), paraffin sections were dewaxed in xylene and rehydrated in decreasing concentrations of ethanol. The primary antibodies and conditions used for IHC are listed in Table 1. Negative controls with no primary antibody were used to assess nonspecific staining. The secondary antibodies used were horseradish peroxidase–conjugated goat anti-rabbit IgG (1:200; Dako, Glostrup, Denmark), rabbit anti-goat IgG (1:200; Dako), or rabbit anti-mouse IgG (1:200; Dako). 3,3′-Diaminobenzidine (Dako) was used as the chromogen. TdT-mediated dUTP-biotin nick-end labeling (TUNEL) staining was performed using the *In situ* Apoptosis Detection Kit (MK500; TaKaRa Bio Inc., Shiga, Japan), according to the manufacturer's protocol. All sections were counterstained with Meyer's hematoxylin.

Quantification of Liver Fibrosis

Morphometric image analysis was performed in liver tissue specimens with a computerized system, consisting of a photomicroscope, a digital camera, and LuminaVision 2.4 bioimaging software (Mitani Corporation, Tokyo, Japan) to quantitatively assess fibrosis. The proportion of the area stained with Sirius red in the liver sections was calculated as the sum of the pixelwise-bound stain measurements divided by the number of summed pixels.

Quantitative Real-Time PCR

Total RNA was extracted from liver and liver tumor tissues using the RNeasy Mini Kit (Qiagen, Valencia, CA). cDNAs were synthesized as previously described. Gene expression was measured by quantitative real-time PCR using cDNA, real-time PCR Master Mix Reagents (Toyobo, Osaka), or TaqMan Fast Universal PCR Master Mix (Applied Biosystems, Foster City, CA), and a set of gene-specific oligonucleotide primers and probes (Table 2) using an Applied Biosystems Prism 7500 (Applied Biosystems). GAPDH levels were measured and used to normalize the relative abundance of mRNA.

Table 2. Primers Used for RT-qPCR

Gene	Sequence
AFP	
Forward	5′-CACACCCGCTTCCCTCAT-3′
Reverse	5′-TTTTCGTGCAATGCTTTGGA-3′
Bcl2	
Forward	5′-AAGGGCTTCACACCCAAATCT-3′
Reverse	5′-CTTCTACGTCTGCTTGGCTTTGA-3′
Cdkn2a	
Forward	5′-GCTCTGGCTTTCGTGAACATG-3′
Reverse	5′-GTGCGGCCCTCTTCTCAA-3′
Cebpα	
Forward	5′-CGCAAGAGCCGAGATAAAGC-3′
Reverse	5′-CGGTCATTGTCACTGGTCAACT-3′
Col1α1	
Forward	5′-GACATCCCTGAAGTCAGCTGC-3′
Reverse	5′-TCCCTTGGGTCCCTCGAC-3′
Cyclin D1	
Forward	5′-GCCCGGAGGGATTTGC-3′
Reverse	5′-AGACGGAACACTAGAACCTAACAGATT-3′
Cyclin D2	
Forward	5′-AAGGCAGATACTCATCAAACACAGA-3′
Reverse	5′-CTGGTGCACGCATGCAA-3′
Fos	
Forward	5′-CCCCAAACTTCGACCATGAT-3′
Reverse	5′-GGAGGATGACGCCTCGTAGTC-3′
GAPDH	
Forward	5′-TGCACCACCAACTGCTTAG-3′
Reverse	5′-GGATGCAGGGATGATGTTC-3′
IL-6	
Forward	5′-CGCTATGAAGTTCCTCTCTGCAA-3′
Reverse	5′-CACCAGCATCAGTCCCAAGA-3′
IL-1β	
Forward	5′-CCATGGCACATTCTGTTCAAA-3′
Reverse	5′-GCCCATCAGAGGCAAGGA-3′
Jun	
Forward	5′-CCGCCCCTGTCCCCTAT-3′
Reverse	5′-TCCTCATGCGCTTCCTCTCT-3′
Pak1	
Forward	5′-CGTATTGCGGGTGTTTGCTA-3′
Reverse	5′-CACAGCAGGAGAACCAAAACC-3′
p53	
Forward	5′-GCATGAACCGCCGACCTAT-3′
Reverse	5′-CAGAAGGTTCCCACTGGAGTCT-3′
Src	
Forward	5′-CCTCCCGCACCCAGTTC-3′
Reverse	5′-CATCAGCATGTTTGGAGTAGTAAGC-3′
TGFβ3	
Forward	5′-AGGGCCCTGGACACCAATTAC-3′
Reverse	5′-CCTTAGGTTCTGGGACCCATTTC-3′
TNFα	
Forward	5′-CCTCACACTCAGATCTTCTCA-3′
Reverse	5′-GCTGCTCCTCCACTTGGTG-3′
Probe	5′-GCAAGCCTGTAGCCCACGTCGTAGCAAA-3′

Immunoblotting

Protein samples (10 to 20 μg) were subjected to SDS-PAGE and transferred to Immobilon P membranes (Millipore Corp, Bedford, MA). After blocking, membranes were probed with primary antibodies against Cygb (1:500) from our laboratory (Table 1), Akt (1:1000; Cell Signaling, Danvers, MA), phosphorylated Akt (1:500; Cell Signaling), extracellular signal–regulated kinase (Erk; 1:500; Cell Signaling), phosphorylated Erk (1:1000; Cell Signaling), cyclin D1 (1:5000; Cell Signaling), nitrotyrosine (1:500; Cell Signaling), or GAPDH (1:2000; Santa Cruz Biotechnology, Santa Cruz, CA). Membranes were

then labeled with horseradish peroxidase–conjugated secondary antibodies. Immunoreactive bands were visualized using the ECL detecting reagent (GE Healthcare UK Ltd, Buckinghamshire, UK) and documented with an LAS 1000 (Fuji Photo Film, Kanagawa, Japan).

Data Analyses

The data presented as bar graphs are the means ± SDs in all experiments. Statistical analyses were performed using the Student's *t*-test, and $P < 0.05$ indicated statistical significance.

Results

Characterization of the Cygb$^{-/-}$ *Mice*

Cygb-deficient mice were generated by deleting exon 1 of the mouse *Cygb* gene (Figure 1A) and backcrossed on the C57BL/6J background. Southern blotting (Figure 1B) and PCR genotyping using mouse tail DNA (data not shown) confirmed the deletion of the *Cygb* gene. Both Cygb mRNA and protein expression were absent in *Cygb*$^{-/-}$ mouse livers, compared with wild-type livers (Figure 1C). Furthermore, IHC indicated that the Cygb protein was present in sinusoidal lining cells in addition to perivascular cells around the portal and central veins, as previously reported,[1] in *Cygb*$^{+/+}$ mice, whereas it was undetected in *Cygb*$^{-/-}$ mice (Figure 1D). Together, these data demonstrate the successful production of the *Cygb*$^{-/-}$ mice.

The mice homozygous for the disrupted allele appeared normal both morphologically and histopathologically 1 month after birth. Next, we examined whether Cygb influenced the toxicity and carcinogenesis of DEN in mice.

Cygb Deficiency Strongly Promotes DEN-Induced Tumorigenesis

DEN is a commonly used chemical carcinogen for the liver because it is activated by cytochrome P-450 enzymes in hepatocytes.[21] C57BL/6J mice were reported to be relatively resistant to liver tumor development under DEN treat-

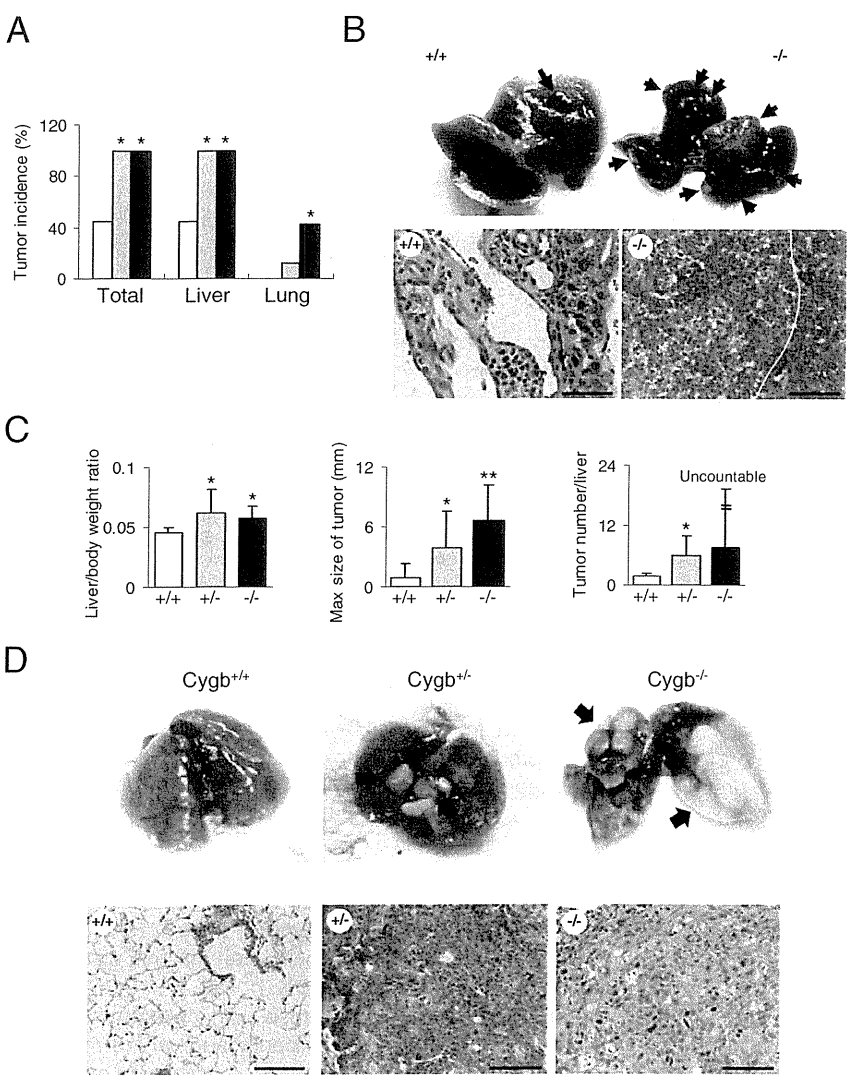

Figure 2. Tumor development in *Cygb*-deficient mice treated with 25-ppm DEN for 25 weeks. **A:** Tumor incidence in total, livers, and lungs from DEN-treated *Cygb*$^{+/+}$ (white bars), *Cygb*$^{+/-}$ (gray bars), and *Cygb*$^{-/-}$ (black bars) mice (n = 7 to 12). $^{*}P < 0.05$ compared with wild type. **B:** Representative gross photographs of livers (**top**) from wild-type (+/+) and *Cygb*-KO (−/−) mice treated with DEN. There was a marked increase in tumor multiplicity in *Cygb*-deficient mice compared with wild-type mice (**arrows**). Representative H&E-stained paraffin sections (**bottom**) of hemangioma from wild-type and poorly differentiated hepatocellular carcinoma composed of small immature neoplastic cells with mitotic figures (the line indicates the boundary of tumor and nontumor areas), from *Cygb*$^{-/-}$ mice. Scale bar = 100 μm. **C:** Determination of liver/body weight ratios, maximum (Max) tumor sizes, and liver tumor numbers for *Cygb*$^{+/+}$ (white bars), *Cygb*$^{+/-}$ (gray bars), and *Cygb*$^{-/-}$ (black bars) mice (n = 7 to 12). Values are given as the mean ± SD. $^{*}P < 0.05$, $^{**}P < 0.01$. **D:** Representative gross photographs (**top**) and microphotographs (**bottom**) of lungs from *Cygb*$^{+/+}$, *Cygb*$^{+/-}$, and *Cygb*$^{-/-}$ DEN-treated mice. Lung tumors were only found in *Cygb*$^{+/-}$ and *Cygb*$^{-/-}$ mice. **Arrows** indicate lung tumors that were classified as squamous cell carcinomas. Scale bar = 100 μm.

ment.[22,23] In this study, we examined whether the loss of Cygb could influence the toxicity and carcinogenesis of DEN in the tumor-resistant C57BL/6J strain. We administered 25-ppm DEN to the drinking water of *Cygb*-deficient male mice at the age of 4 weeks. Unexpectedly, as early as 25 weeks after DEN treatment, 100% of $Cygb^{-/-}$ and $Cygb^{+/-}$ mice developed tumors in the liver and lungs, whereas the tumor incidence in wild-type mice was 44.4% (Figure 2, A and B). The liver/body weight ratio was approximately 50% more than in wild-type animals (Figure 2C) because of these tumor masses. $Cygb^{-/-}$ mice displayed significantly larger lesions and produced tumors more frequently than wild-type mice (Figure 2C).

DEN has induced tumors in the liver and in the lungs of the B6C3F1 mouse strain, although with a lower frequency.[24] Consistent with these studies, lung tumors were found in $Cygb^{+/-}$ and $Cygb^{-/-}$ mice, with a frequency of 11.7% and 57.1%, respectively, whereas $Cygb^{+/+}$ mice showed complete resistance (Figure 2, A and D).

Next, using a low dose of DEN, at which wild-type mice do not develop liver tumors, we examined whether *Cygb* deficiency functioned as a tumor promoter. We took advantage of earlier observations that, when DEN was administered to mice at a nontoxic dose, it failed to induce liver cancer, unless combined with a tumor promoter, such as phenobarbital.[25,26] We maintained wild-type and *Cygb*-deficient male mice during DEN administration at the nontoxic dose of 0.05 ppm for 36 weeks. As a result, >40% of $Cygb^{-/-}$ mice developed tumors in the liver or lungs, whereas, as expected, wild-type mice exhibited no tumor formation (Figure 3). $Cygb^{+/-}$ mice showed an intermediate sensitivity. These findings confirm the tumor-promoting effects of *Cygb* depletion.

To define the histological features of the liver tumors, liver samples were evaluated IHC. The liver tumors in C57BL/6 mice (wild type) administered DEN in drinking water were dominantly composed of cholangiomas, hemangiomas, hemangiosarcomas, and, to a lesser degree, hepatocellular carcinomas.[27–29] In this study, *Cygb*-deficient and wild-type mice developed similar histological alterations in the liver, including hemangioma (Figure 2B), hepatocellular carcinoma (Figures 2B and 3B), which stained positive for alpha-fetoprotein (AFP) (Figure 4A), and cholangioma, which stained positive for CK19 (Figure 4A). Quantitative real-time PCR (RT-qPCR) analysis showed increased mRNA expression of AFP in $Cygb^{+/-}$ and $Cygb^{-/-}$ mice compared with their wild-type counterparts (Figure 4B).

In the liver, Cygb was present in stellate cells.[1,4] We used cellular retinol-binding protein-1 and α-smooth muscle actin antibodies to detect stellate cell expression. The presence of cellular retinol-binding protein-1– and α-smooth muscle actin–expressing cells in the liver parenchyma from DEN-treated homozygote mice indicated that stellate cells were present along sinusoids, even in the absence of Cygb (Figure 4C). The expression of α-smooth muscle actin and desmin, another marker of stellate cells, was markedly augmented in $Cygb^{-/-}$ mice (Figure 4C). Next, we assessed whether liver fibrosis developed in these mice. Sirius red staining for collagen deposition in paraffin-embedded sections of liver samples

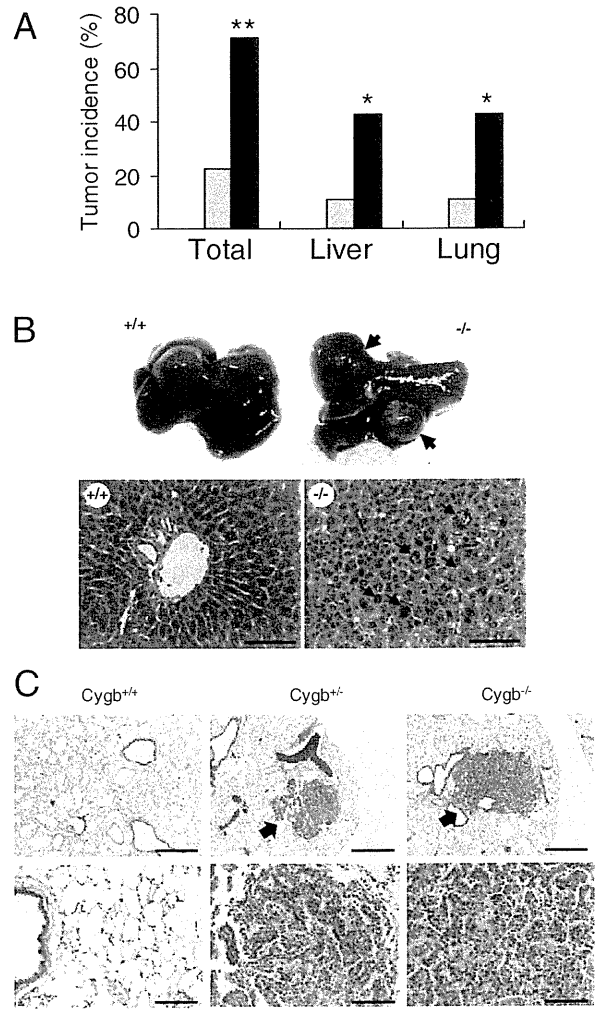

Figure 3. Tumor development in *Cygb*-deficient mice treated with 0.05-ppm DEN for 36 weeks. **A:** Tumor incidence in total, livers, and lungs from 0.05-ppm DEN-treated $Cygb^{+/+}$ (white bars), $Cygb^{+/-}$ (gray bars), and $Cygb^{-/-}$ (black bars) mice (n = 7 to 15). $^{*}P < 0.05$, $^{**}P < 0.01$ compared with the wild type. **B:** Gross photographs of livers (**top**) from $Cygb^{+/+}$ and $Cygb^{-/-}$ mice treated with 0.05-ppm DEN, as previously mentioned; **arrows** indicate lung tumors. Representative photomicrographs of H&E-stained paraffin sections of liver parenchyma (**bottom**) from wild-type and moderately differentiated hepatocellular carcinoma composed of large cells that vary in size and shape (**arrows**), from $Cygb^{-/-}$ mice. Scale bar = 100 μm. **C:** Representative photomicrographs of H&E-stained paraffin sections of lungs from $Cygb^{+/+}$, $Cygb^{+/-}$, and $Cygb^{-/-}$ mice treated with 0.05-ppm DEN for 36 weeks. Scale bars: 400 μm (**top**); 100 μm (**bottom**). **Arrows** indicate lung tumors that were classified as adenocarcinomas. No lung tumor was observed in $Cygb^{+/+}$ mice.

collected from $Cygb^{+/+}$ and $Cygb^{-/-}$ mice treated with 25-ppm DEN for 25 weeks showed marked deposition of collagen (red) around the hepatocytes (pericellular fibrosis) in $Cygb^{-/-}$ mice (Figure 4D). Morphometric image analysis was performed with a computerized system, consisting of a photomicroscope, a digital camera, and LuminaVision 2.4 bioimaging software, to quantitatively assess fibrosis. The Sirius red–positive area of $Cygb^{-/-}$ mice (7.67% ± 7.82%, n = 3) was significantly greater than that in $Cygb^{+/+}$ mice (mean ± SD, 1.36% ± 0.36%, n = 3; $P < 0.05$, Kruskal-Wallis test). Pericellular fibrosis with collagen deposition was accompanied by significantly augmented mRNA expression of collagen 1α1 and tissue inhibitor of matrix met-

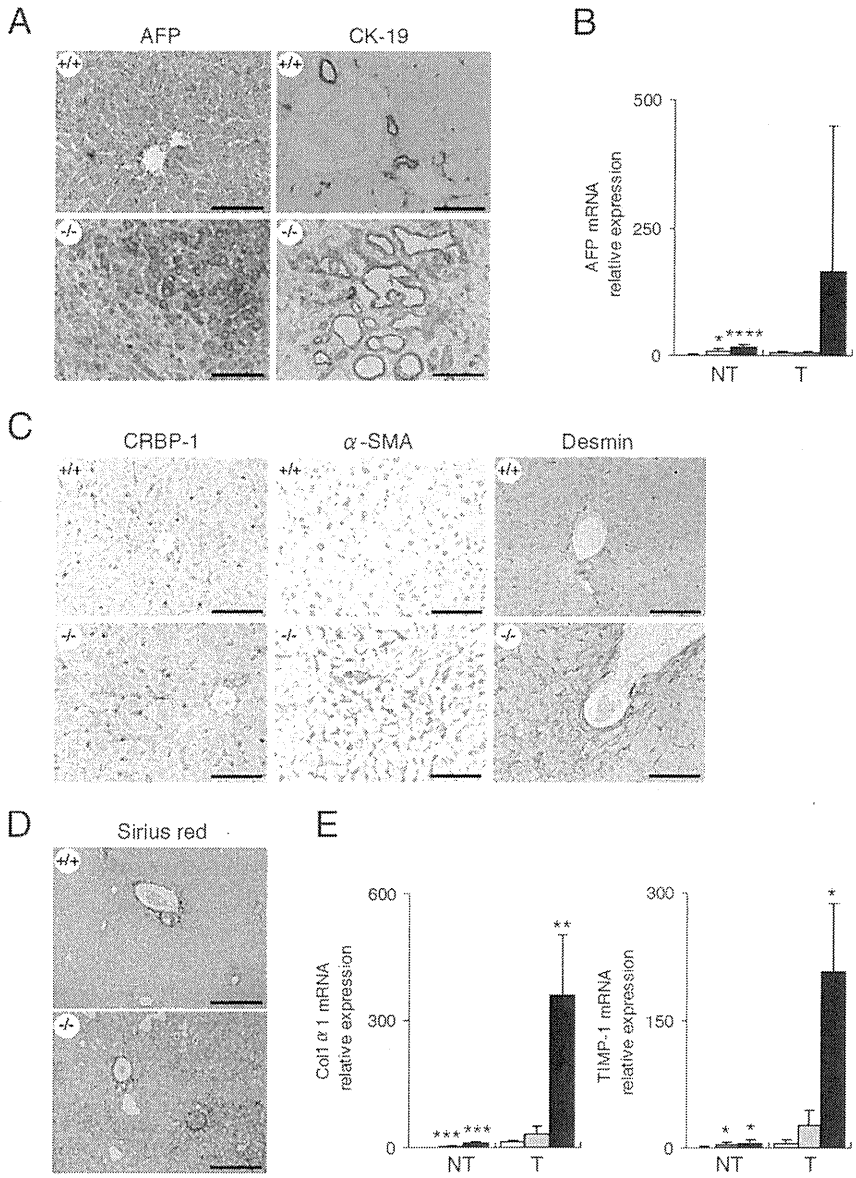

Figure 4. Expression of tumor markers and liver fibrosis development in DEN-treated *Cygb*-deficient mice. *Cygb*-deficient mice from Figure 2 were subjected to histological and biochemical analyses. **A:** Paraffin-embedded liver sections from $Cygb^{+/+}$ and $Cygb^{-/-}$ mice were stained with AFP and cytokeratin 19 (CK-19). Scale bar = 100 μm. **B:** Expression of AFP mRNA in $Cygb^{+/+}$ (white bars), $Cygb^{+/-}$ (gray bars), and $Cygb^{-/-}$ (black bars) mice livers was determined by RT-qPCR (n = 7 to 12). Levels were normalized to GAPDH. Values are given as the mean ± SD of all experiments. NT, nontumor area; T, liver tumor. $^{*}P < 0.05$, $^{****}P < 0.0001$. **C:** Paraffin-embedded liver sections were IHC stained for the detection of CRBP-1, α-SMA, and desmin. Scale bar = 100 μm. **D** and **E:** Development of liver fibrosis. **D:** Sirius red staining for collagen deposition in paraffin-embedded liver sections. Scale bar = 100 μm. There was marked deposition of collagen (red) around the hepatocytes (pericellular fibrosis) in $Cygb^{-/-}$ mice. **E:** Relative levels of collagen (Col) 1α1 and tissue inhibitor of matrix metalloproteinase-1 (TIMP-1) mRNA in the nontumor area (NT; n = 7 to 12) and in liver tumors (T; n = 3 to 5) of $Cygb^{+/+}$ (white bars), $Cygb^{+/-}$ (gray bars), and $Cygb^{-/-}$ (black bars) mice were determined by RT-qPCR and normalized to GAPDH mRNA. Values are given as the mean ± SD of all experiments. $^{*}P < 0.05$, $^{**}P < 0.01$, and $^{***}P < 0.001$.

taloproteinase-1 in the livers of $Cygb^{-/-}$ mice, compared with that of $Cygb^{+/+}$ mice treated with 25-ppm DEN for 25 weeks (Figure 4E). Thus, the augmented occurrence of pericellular fibrosis and fibrotic reactions in *Cygb* deficiency may be involved in the development of liver cancer.

Cygb *Loss Is Associated with Increased Cancer Cell Proliferation*

Two important cellular processes in tumorigenesis are cell apoptosis and proliferation. To examine how *Cygb* loss affected these two processes in the livers of C57BL/6J mice, we determined the labeling indexes of TUNEL, as a marker of apoptotic cells, and proliferating cell nuclear antigen (PCNA), as a marker of proliferating cells in the liver, both in the tumor and adjacent nontumor areas of $Cygb^{+/+}$ and $Cygb^{-/-}$ mice treated with 25-ppm DEN in drinking water for 25 weeks. Liver tumors in $Cygb^{-/-}$ mice exhibited reduced apoptotic cell death relative to liver tumors in $Cygb^{+/+}$ mice (Figure 5, A and C) and showed elevated mRNA expression of the antiapoptotic protein Bcl-2 (Figure 5E). Liver tumors in the $Cygb^{-/-}$ mice exhibited more proliferating cells than the tumors of the wild-type mice, as shown by PCNA labeling (Figure 5, B and D), in addition to elevated cyclin D1 mRNA expression (Figure 5F). These results suggest that stimulation of proliferating neoplastic cells is the primary cellular mechanism for increased liver tumorigenesis in *Cygb*-deficient mice.

Cygb-*Deficient Mice Exhibit Elevated Phosphorylated Akt and Erk and Liver Inflammation*

To identify the signaling pathways responsible for enhanced hepatocyte survival and proliferation, we ex-

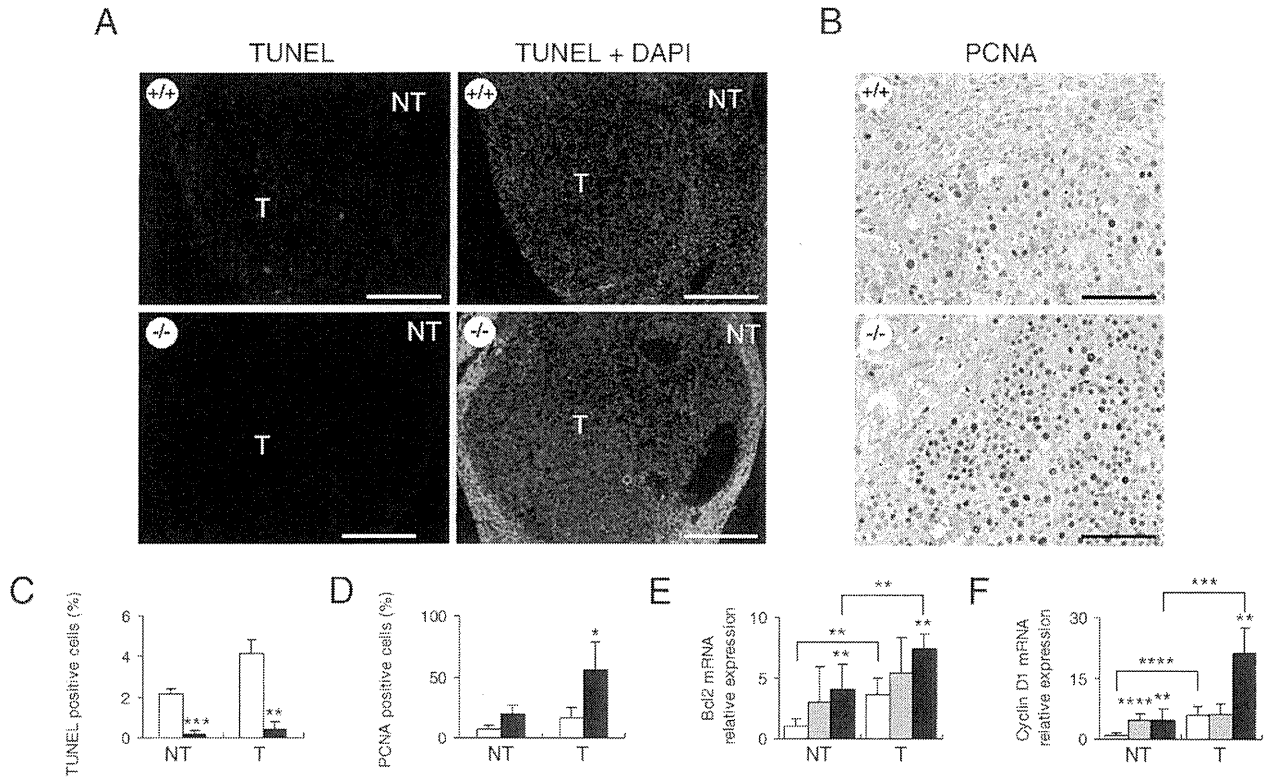

Figure 5. Tumor-bearing *Cygb*-deficient mice are associated with increased cancer cell proliferation and reduced apoptosis. **A:** Paraffin-embedded liver sections from wild-type (+/+) and homozygous (−/−) mice treated with 25-ppm DEN for 25 weeks were TUNEL labeled (**left**) and counterstained with DAPI (**right**). Apoptotic cells were present in the tumor (T) area in wild-type mice. NT, nontumor area. Scale bar = 400 μm. **B:** Paraffin-embedded liver sections were stained with PCNA. Scale bar = 100 μm. The frequency of apoptotic (**C**) or proliferate (**D**) cells was determined by counting TUNEL- or PCNA-positive cells, respectively (cells with the nucleus stained dark brown in the case of PCNA), in at least 1000 cells from each liver ($n = 3$). Expression levels of Bcl-2 (**E**) and cyclin D1 (**F**) mRNA in the NT ($n = 7$ to 12) and T ($n = 3$ to 5) areas from 25-ppm DEN-treated mice were determined by RT-qPCR and normalized to GAPDH. $Cygb^{+/+}$ (white bars), $Cygb^{+/-}$ (gray bars), and $Cygb^{-/-}$ (black bars) mice. Values are given as the mean ± SD of all experiments. $^{*}P < 0.05$, $^{**}P < 0.01$, $^{***}P < 0.001$, and $^{****}P < 0.0001$.

amined the effects of *Cygb* deficiency on the major pathways implicated in liver cancer.[30] As expected, *Cygb* loss was associated with an increase in both Akt phosphorylation and abundance in the livers (Figure 6A). This observation was also evident for Erk signaling (Figure 6, A and B). Consistent with increased Erk phosphorylation, *Cygb*-deficient mice exhibited increased expression of cyclin D1 (Figure 6A), and Jun and Fos mRNA in nontumor and tumor areas, relative to wild type (Figure 6C). These results suggested that the Akt and Erk pathways are activated in response to *Cygb* deficiency. The increased levels of Akt and Erk activation correlated with a marked elevation of IL-6 mRNA in both nontumor and tumor areas in *Cygb*-deficient mice (Figure 6D). IL-6 is a tumor-promoting cytokine that is required for Erk activation and contributes to alterations in Akt signaling.[31] Knowing that IL-6 functions as a downstream mediator for both IL-1 and tumor necrosis factor-α,[32] we examined the expression of these two cytokines. Remarkably, IL-1β and Tnfα levels (Figure 6D) increased 10- and 30-fold, respectively, at the mRNA level in the nontumor area of the liver and increased further in the tumors, relative to wild type. *Cygb*-deficient mice also had increased expression of Tgfβ3 mRNA (Figure 6D). These data suggest that *Cygb* loss can trigger inflammation and lead to the long-term elevation of tumor-promoting cytokines, resulting in the development of tumors.

Nitrotyrosine Accumulation in the Livers of DEN-Treated Cygb*-Deficient Mice*

Long-term administration of DEN has induced the expression of the inducible isoform of NO synthase and 3-nitrotyrosine, a marker of peroxynitrite formation, in preneoplastic and neoplastic rat liver tissues.[33] In this study, we detected the overproduction of nitrotyrosine in tumor and nontumor liver tissues of *Cygb*-deficient mice, compared with wild-type mice, as shown by IHC (Figure 7A) and immunoblot analyses (Figure 7B). These results indicate the high production of NO, together with superoxide, in *Cygb*-deficient mice.

Dysregulation of Genes Associated with Cell Proliferation and Differentiation in Cygb*-Deficient Mice*

To further screen for cellular alterations caused by *Cygb* gene disruption, we compared gene expression profiles between *Cygb*-deficient mice and their wild-type counterparts after 25-ppm DEN treatment for 25 weeks. We

observed the altered expression of cancer genes, including p53, cyclin D2, Pak1 (p21-activated kinase), Src, Cdkn2a, and Cebpa (CCAAT/enhancer-binding protein α) (data not shown). We examined in detail the mRNA levels of these genes by RT-qPCR. Consistent with the high rate of cellular proliferation in the liver of *Cygb*-deficient mice (Figure 5, B and D), we observed overexpression of cyclin D2 (Figure 8A) and p53 (Figure 8B), which have displayed high expression in astrocytomas, a type of brain tumor.[34] Pak1 promotes malignant tumor progression, and the Src proto-oncogene has shown increased expression in human skin tumors and leukemia.[35–38] In this study, we found that the mRNA expression of Pak1, in addition to Src, increased fivefold in the livers of $Cygb^{-/-}$ mice, relative to the wild type (Figure 8, C and D).

Cdkn2a, a tumor suppressor that negatively regulates the cell cycle, displayed increased expression at the mRNA level in the livers of *Cygb*-deficient mice (Figure 8E), consistent with other studies[39,40] on sarcomas and lung tumors.

Cebpa has the ability to inhibit proliferation, particularly in hepatocytes.[41,42] Down-regulation of CEBPA has been reported in human myeloid leukemia.[43] Consistent with these studies, our results showed decreased expression of Cebpa mRNA in the liver of *Cygb*-deficient mice, relative to the wild type (Figure 8F).

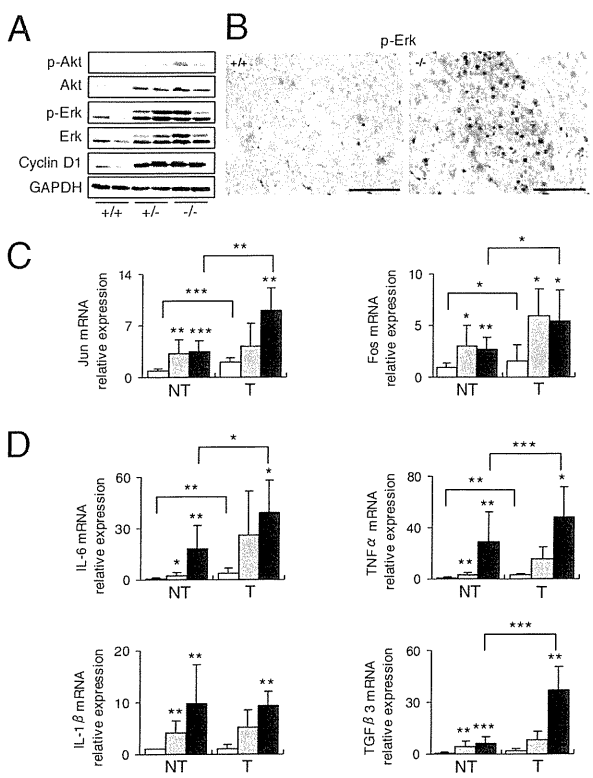

Figure 6. Tumor-bearing *Cygb*-deficient mice exhibited elevated phosphorylated Akt (p-Akt), phosphorylated Erk (p-Erk), and inflammation. *Cygb*-deficient mice from Figure 2 were subjected to additional biochemical and gene expression analyses. **A:** The liver was lysed and gel separated, and the levels of p-Akt, p-Erk, total Akt, total Erk, and cyclin D1 were examined by immunoblot analyses. All blots were reprobed with anti-GAPDH as a loading control. **B:** Paraffin-embedded liver sections were stained for phosphorylated Erk. Scale bar = 100 μm. **C** and **D:** Relative mRNA levels of Jun and Fos (**C**) and IL-6, Tnfα, IL-1β, and Tgfβ3 (**D**) in the nontumor (NT; n = 7 to 12) and tumor (T; n = 3 to 5) areas of the liver were determined by RT-qPCR and normalized to GAPDH. $Cygb^{+/+}$ (white bars), $Cygb^{+/-}$ (gray bars), and $Cygb^{-/-}$ (black bars) mice. Values are given as the mean ± SD of all experiments. $^{*}P < 0.05$, $^{**}P < 0.01$, and $^{***}P < 0.001$.

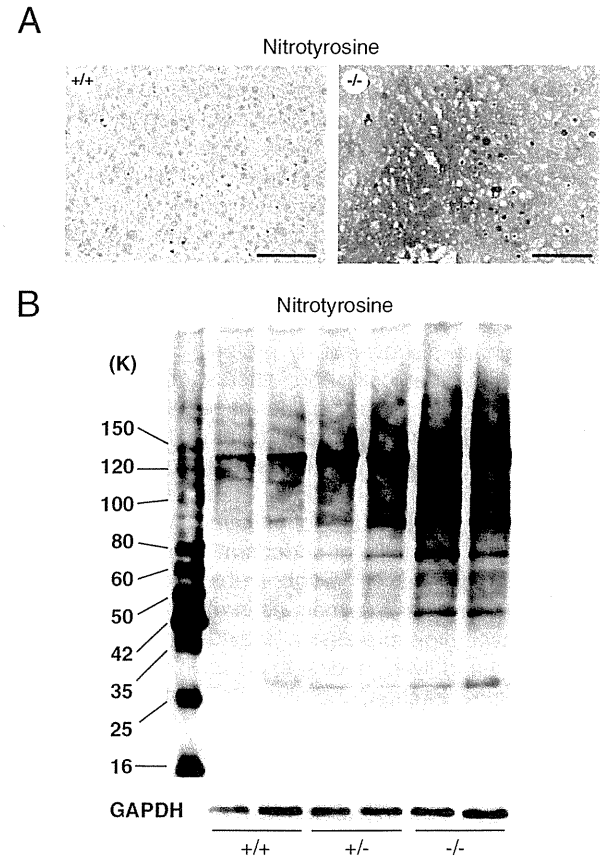

Figure 7. Peroxynitrite formation in the livers of *Cygb*-deficient mice. **A:** Paraffin-embedded liver sections from wild-type (+/+) and homozygous (−/−) mice treated with 25-ppm DEN for 25 weeks were stained with antinitrotyrosine. Nitrotyrosine-containing proteins were strongly expressed in the cytoplasm and nuclei of cancer cells in the tumor area, particularly in the inclusions of cancer cells. Scale bar = 100 μm. **B:** Protein homogenates of liver tissues from $Cygb^{+/+}$, $Cygb^{+/-}$, and $Cygb^{-/-}$ mice treated with 25-ppm DEN for 25 weeks were subjected to immunoblot detection for nitrotyrosine. GAPDH was used as a loading control. K, kDa (molecular mass).

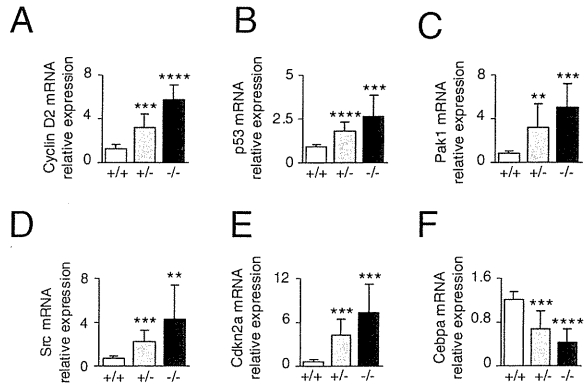

Figure 8. Altered regulation of cancer genes in *Cygb*-deficient mice. RT-qPCR analysis of cell growth–related gene transcripts cyclin D2 (**A**), p53 (**B**), and Pak1 (**C**) and cell differentiation and apoptosis-related gene transcripts Src (**D**), Cdkn2a (**E**), and Cebpa (**F**) in liver from mice treated with 25-ppm DEN for 25 weeks (n = 7 to 12). Levels are normalized to GAPDH. $Cygb^{+/+}$ (white bars), $Cygb^{+/-}$ (gray bars), and $Cygb^{-/-}$ (black bars) mice. Values are given as the mean ± SD of all experiments. $^{**}P < 0.01$, $^{***}P < 0.001$, and $^{****}P < 0.0001$.

Discussion

In the present study, we showed that loss of *Cygb* in C57BL/6J mice markedly increased their susceptibility to DEN-induced tumorigenesis. In the absence of *Cygb*, liver tumors developed earlier, were larger, and were more numerous compared with wild-type mice. By administering low-dose DEN to adult mice (0.05 ppm), which failed to induce liver cancer in wild-type mice, we observed the tumor-promoting effects of *Cygb* deficiency.

We observed high levels of Cygb expression in hepatic stellate cells, a liver-specific pericyte, from which Cygb was originally discovered by proteomic analysis of primary cultured rat cells and other stromal cells in the visceral organs, including the pancreas, gut, spleen, lung, and kidney.[1,4] These stromal cells are pericytes localized around the capillaries of the organs that are capable of vitamin A storage. Thus, we propose that Cygb may be an indicator of a vitamin A–storing phenotype of myofibroblasts of endoderm origin. However, as previously reported,[1,4,5] Cygb is ubiquitously expressed in all body organs in human, as in mice and rats. At the mRNA level, high expression is evident in the adult human heart and liver; modest expression is evident in the brain, kidney, trachea, and placenta; and low expression is evident in the adult skeletal muscle.[44] Several cancer cell lines, including HepG2 cells,[44] the NCI-H2228 lung cancer cell line, and HCC 1569 breast cancer cells,[19] also display CYGB mRNA expression. These observations indicate the role of Cygb in the regulation of cellular function originating from the epithelia. In this context, cancer development in the liver and lungs in $Cygb^{-/-}$ mice is anticipated. However, the role of mesenchymal cells that express Cygb highly in tumor development should be further evaluated because these myofibroblasts represent important environmental factors during tumor formation.

Cygb expression is augmented under hypoxia in the liver, heart, brain, and skeletal muscle and in HN33 cells (an immortalized mouse hippocampal cell line), BEAS-2B cells (a transformed human bronchial epithelial cell line), and HeLa cells (a human cervix carcinoma cell line).[16] Overexpression of Cygb protects mouse neuroblastoma N2a cells and human neuroblastoma SH-SY5Y cells under H_2O_2 exposure and the human neuronal cell line TE671 under prooxidant Ro19-8022 stimulation.[11,12,44] Overexpression of Cygb in the liver, induced by adeno-associated–virus-induced transfection, protects the liver from oxidative injury.[13] Conversely, the role of Cygb as an NO scavenger in rat hepatocytes and NIH3T3 fibroblasts may protect cells from NO-induced toxicity.[8,33] These reports and our findings regarding the accumulation of nitrotyrosine protein adducts in *Cygb*-deficient mice indicate the cytoprotective and antioxidative properties of Cygb.

Several tumor suppressor genes are located in both arms of chromosome 17. *TP53*, a known tumor suppressor gene at 17p13.1, is one of the most frequently mutated genes in cancers, including hepatocellular carcinoma.[45] *BRCA1* (breast cancer 1, early onset) at 17q12 is a human tumor suppressor gene encoding the breast cancer type 1 susceptibility protein,[46] which is present in the breast and other tissues, aiding the repair of damaged DNA and the destruction of the cell when DNA cannot be repaired. If *BRCA1* is damaged, cells duplicate uncontrollably, leading to cancer. Other known breast cancer–associated genes include *septin*, *DMC1*, and *HER2/ErbB2*.[47,48] Because *CYGB* exists on chromosome 17q25, genes on this chromosome appear commonly in the tumorigenesis of epithelial cells and mutation or epigenetic modification of these genes appears to trigger malignant transformation.

Clinically, liver cancer develops from a fibrotic liver, with chronic trauma induced by alcohol abuse and hepatitis virus B/C infection.[49] Chronic inflammation offers an appropriate environment for cancer development, by producing multiple growth factors, extracellular matrices, and neovascularization involving local hypoxia.[50] In this context, the augmented occurrence of pericellular fibrosis and fibrotic reactions (Figure 4, C–E) in *Cygb* deficiency may be involved in the development of liver cancer.

In conclusion, to our knowledge, this is the first report that *Cygb* deficiency induces susceptibility to cancer development in the liver and lungs of mice receiving DEN treatment. Thus, *Cygb*-deficient mice may provide a useful animal model to study cancer development in the liver and lungs; globins, such as Cygb, may shed new light on the biological features of organ carcinogenesis.

Acknowledgment

We thank Drs. Masaru Enomoto, Hideki Fujii, and Thoru Komiya for their valuable comments during this study.

References

1. Kawada N, Kristensen DB, Asahina K, Nakatani K, Minamiyama Y, Seki S, Yoshizato K: Characterization of a stellate cell activation-associated protein (STAP) with peroxidase activity found in rat hepatic stellate cells. J Biol Chem 2001, 276:25318–25323
2. Burmester T, Ebner B, Weich B, Hankeln T: Cytoglobin: a novel globin type ubiquitously expressed in vertebrate tissues. Mol Biol Evol 2002, 19:416–421
3. Sawai H, Kawada N, Yoshizato K, Nakajima H, Aono S, Shiro Y: Characterization of the heme environmental structure of cytoglobin, a fourth globin in humans. Biochemistry 2003, 42:5133–5142
4. Nakatani K, Okuyama H, Shimahara Y, Saeki S, Kim DH, Nakajima Y, Seki S, Kawada N, Yoshizato K: Cytoglobin/STAP, its unique localization in splanchnic fibroblast-like cells and function in organ fibrogenesis. Lab Invest 2004, 84:91–101
5. Shigematsu A, Adachi Y, Matsubara J, Mukaide H, Koike-Kiriyama N, Minamino K, Shi M, Yanai S, Imamura M, Taketani S, Ikehara S: Analyses of expression of cytoglobin by immunohistochemical studies in human tissues. Hemoglobin 2008, 32:287–296
6. Sugimoto H, Makino M, Sawai H, Kawada N, Yoshizato K, Shiro Y: Structural basis of human cytoglobin for ligand binding. J Mol Biol 2004, 339:873–885
7. Li RC, Lee SK, Pouranfar F, Brittian KR, Clair HB, Row BW, Wang Y, Gozal D: Hypoxia differentially regulates the expression of neuroglobin and cytoglobin in rat brain. Brain Res 2006, 1096:173–179
8. Fordel E, Geuens E, Dewilde S, Rottiers P, Carmeliet P, Grooten J, Moens L: Cytoglobin expression is upregulated in all tissues upon hypoxia: an in vitro and in vivo study by quantitative real-time PCR. Biochem Biophys Res Commun 2004, 319:342–348
9. Guo X, Philipsen S, Tan-Un KC: Study of the hypoxia-dependent regulation of human CYGB gene. Biochem Biophys Res Commun 2007, 364:145–150